Journal of Sound and Vibration (2000) **231**(2), 343–374
doi:10.1006/jsvi.1999.2719, available online at http://www.idealibrary.com on IDEAL®

AN INVESTIGATION IN STIFFNESS EFFECTS ON DYNAMICS OF ROTOR–BEARING–FOUNDATION SYSTEMS

Y. KANG, Y.-P. CHANG, J.-W. TSAI, L.-H. MU AND Y.-F. CHANG

Department of Mechanical Engineering, Chung Yuan Christian University, Chung Li, Taiwan 32023, *Republic of China*

(*Received* 3 *September* 1996, *and in final form* 20 *September* 1999)

This paper is devoted to the study of foundation effects on the dynamic characteristics of rotor-bearing systems. The modelling and analysis of rotor-bearing–foundation systems based on the finite element method are discussed. A substructure procedure which includes the foundation effects in the motion equations and the application of the dynamic solver of a commercial package is addressed. The design criteria of the foundation for rotating machinery avoiding resonance and suppressing response have also been emphasized through numerical examples.

1. INTRODUCTION

High-speed and light-weight are two features of rotating machinery demanded in modern applications. Thus, accurate predictions of critical speeds, whirl responses and modal characteristics are necessary for safe operations. Typical rotor-bearing system models cannot insure accurate solutions because the foundation effects are ignored.

Various studies have incorporated foundation effects in a rotor-bearing system analysis. Kirk and Gunter [1] analyzed the steady state and transient responses of the Jeffcott rotor for elastic bearings mounted on damped and flexible supports. They disregarded the rotor flexibility and the disk gyroscopic effects in the formulation of the governing equations of motion, and provided design charts for both turned and off-turn support conditions to minimize the foundation characteristics of the rotor amplitude and force transmitted over a given speed range. Smith [2] investigated the Jeffcott rotor with internal damping to include a massless, damped and flexible support system. Lund [3] and Gunter [4] showed that damped and flexible supports may improve the stability of high-speed rotors. Also, Lund and Sternlicht [5], Dworski [6], and Gunter [7] demonstrated that a significant reduction in the transmitted force could be achieved by the proper design of a bearing support system. Pilkey *et al.* [8] presented an efficient two-stage procedure for optimizing suspension systems of rotors. From these studies, the dynamic performance problems in association with the foundation

0022-460X/00/120343 + 32 $35.00/0

effects on mass, damping, and stiffness of the well-known Jeffcott rotor incorporating the bearing support systems could be found.

Gasch [9] dealt with the flexible rotating shaft of a large turbo-rotor by the finite element analysis. He introduced foundation dynamics into the rotor equations via receptance matrices, which were obtained from modal testing and modal analysis. Vance *et al.* [10] provided comparison results for computer predictions and experimental measurements on a rotor-bearing test apparatus. They have modelled the rotor-bearing system to include foundation impedance effects by using the transfer matrix method. Stephenson and Rouch [11] have utilized the finite element method to analyze rotor-bearing–foundation systems. They provided a procedure using modal analysis techniques, which could be applied in measuring frequency response functions to include the dynamic effects of the foundation structure.

Many finite element procedures developed for rotor-bearing systems have been implemented toward generalizing and improving the formulation, such as by Ruhl and Booker [12]. In this early investigation, the effects of rotary inertia, gyroscopic moments, shear deformation, axial load, and internal damping have been neglected. Nelson and McVaugh [13] have utilized the Rayleigh beam finite element to formulate the rotor-bearing systems by including the additional effects as mentioned above. Zorzi and Nelson [14] in 1977 and 1980 [15] worked on the generalization of a similar model by including internal damping and axial torque respectively. Nelson [16] and Greenhill *et al.* [17] utilized Timoshenko beam shape functions to establish the shaft element formulation. Özgüven and Özkan [18] further improved the shaft finite element model by including the effect of internal hysteric and viscous damping. There are many software packages available today for analyzing whirl responses, and predicting stability and modal characteristics of rotor-bearing systems [19, 20]. However, the packages are designed for particular usage of rotor-bearing systems their use may be limited if the involved foundation is very complex.

It is known that the foundation can have a significant effect on the dynamics of rotor-bearing systems. The mathematical model of foundation structure is essentially utilized to update the motion equations of rotor-bearing–foundation systems. This study shows how to apply a commonly used package to analyze the dynamic characteristics of rotor-bearing–foundation systems. The analysis extends the finite element models to include large degree of freedom (d.o.f.) of the rotor-bearing system and complex foundation structure. Also, a two-node element provided by the package to model disk, bearing and suspension is emphasized. In the numerical examples, the effects of both lumped-mass and continuous foundations are evaluated.

2. FINITE ELEMENT MODELLING OF SUBSTRUCTURES

As shown in Figure 1, the overall system of a typical rotating machine may be divided into five subsystems; namely, the shaft, the rotating disk, the bearing, the foundation structure, and the suspension. Each subsystem is modelled in turn, and then these subsystems are combined by using compatibility conditions along with the common co-ordinates to give an overall system model.

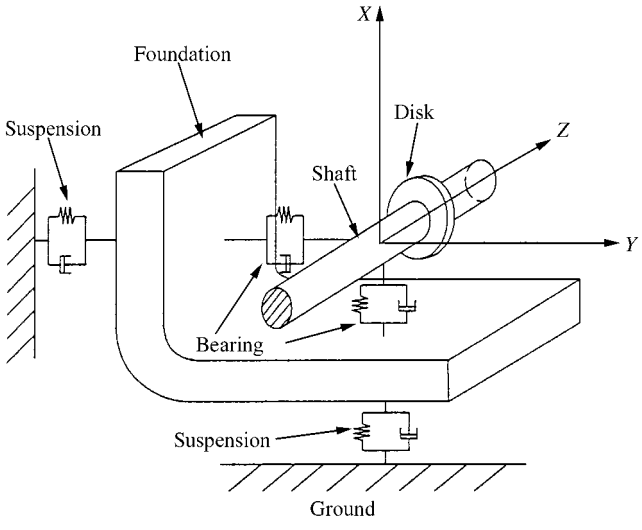

Figure. 1. The model of rotor-bearing–foundation system.

Other features such as coupling between two shafts in series, vibration isolator, vibration absorber and control actuators for vibration suppression may eventually be superimposed onto the overall system model. Since these are beyond the scope of this paper, they are not to be considered here.

The rotor system is idealized as a system consisting of a large number of finite shaft elements of circular cross-section with rigid disks mounted at one end or both the ends of some shaft elements. In addition to the shaft elements, this system has bearings, i.e., the non-isotropic fluid film or isotropic rolling bearing type. The structure beyond the bearing is the foundation that includes the bearing housing and the machine support structure.

For a shaft element provided by the ANSYS library [21], the d.o.f. are defined by $\{q\} = (u_x, u_y, u_z, \theta_x, \theta_y, \theta_z)^{\mathrm{T}}$. Each element is modelled by 12 d.o.f.s with two lateral translations (u_x, u_y), one axial translation (u_z), two bending rotations (θ_x, θ_y), and one twisting rotation (θ_z) at each node. In the stationary frame of reference, the equation of motion for the whole shaft which excludes all disks and bearings can be written in a general form as

$$[M^e]\{\ddot{q}\} + ([C^e] + \Omega[G^e])\{\dot{q}\} + [K^e]\{q\} = \Omega^2\{F_u^e\} + \{F_g^e\} + \{Q^b\} + \{Q^d\}, \quad (1)$$

where $\{F_u^e\}$ is the vector of unbalance forces, $\{F_g^e\}$ is the vector of unidirectional load of shaft and $\{Q^d\}$, $\{Q^b\}$ are the vectors of interactive forces at nodes of disk locations and bearing locations respectively.

The disks without the length effect as shown in Figure 2 are modelled by a two-node element including mass, rotary inertia, and gyroscopic moment. The d.o.f. of this two-node element is the same as that of a shaft element. The governing equation is expressed as follows:

$$[M^d]\{\ddot{q}^d\} + \Omega[G^d]\{\dot{q}^d\} = \Omega^2\{F_u^d\} + \{F_g^d\} - \{Q_d^e\} + \{Q_d^g\}, \quad (2)$$

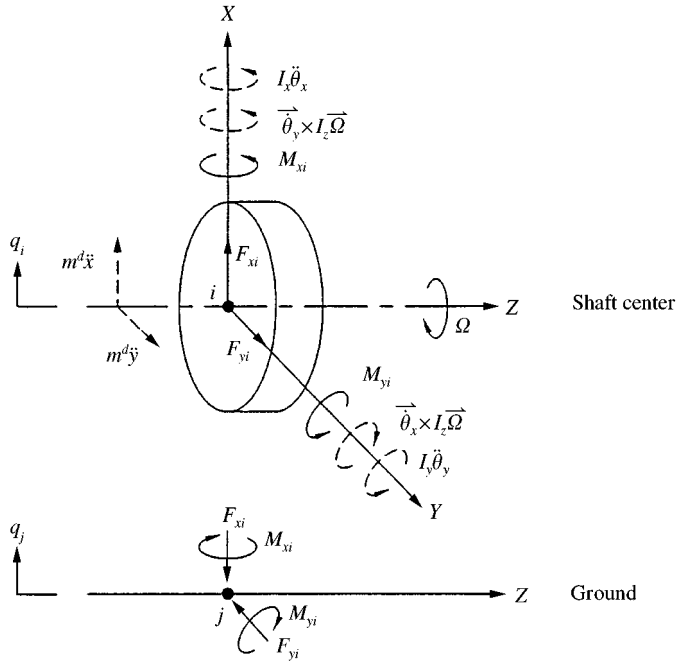

Figure. 2. The two-node model of a disk.

where $\{F_u^d\}$ and $\{F_g^d\}$ are the vectors of unbalance forces and unidirectional load respectively, $\{Q_d^e\}$ is a vector of interaction forces and moments at the common nodes of the disk and the shaft, $\{Q_d^g\}$ is a vector of inertia forces and inertia moments of the disk relative to the ground. The details of disk model are shown in Appendix A. In the equations expressed above, rotating symmetry is assumed for the finite shaft elements and the rigid disks.

Figure 3(a) and 3(b) show the simplified models of a bearing on a continuous-mass and flexible foundation and a suspension of the same foundation respectively. Similarly, with the length effects of the bearing being neglected, an eight-coefficient model including direct and cross-effects of stiffness and damping properties may be used to model the bearings. In this model, the interactive force acting at each bearing is obtained from

$$[C^b]\{\dot{q}^b\} + [K^b]\{q^b\} = -\{Q_b^e\} + \{Q_b^f\}, \tag{3}$$

where $\{Q_b^f\}$ is the vector of interactive forces and moments at the common nodes of bearings and foundation; $\{q^b\}$ includes the common nodes of shaft and bearing and those of bearing and foundation.

Similarly, the interactive forces acting at each suspension are obtained by

$$[C^s]\{\dot{q}^s\} + [K^s]\{q^s\} = -\{Q_s^f\} + \{Q_s^g\}, \tag{4}$$

where $\{Q_s^f\}$ and $\{Q_s^g\}$ are interactive forces at the common nodes of suspension and foundation, and of suspension and ground respectively. The details of the bearing model and the suspension model are also shown in Appendix A.

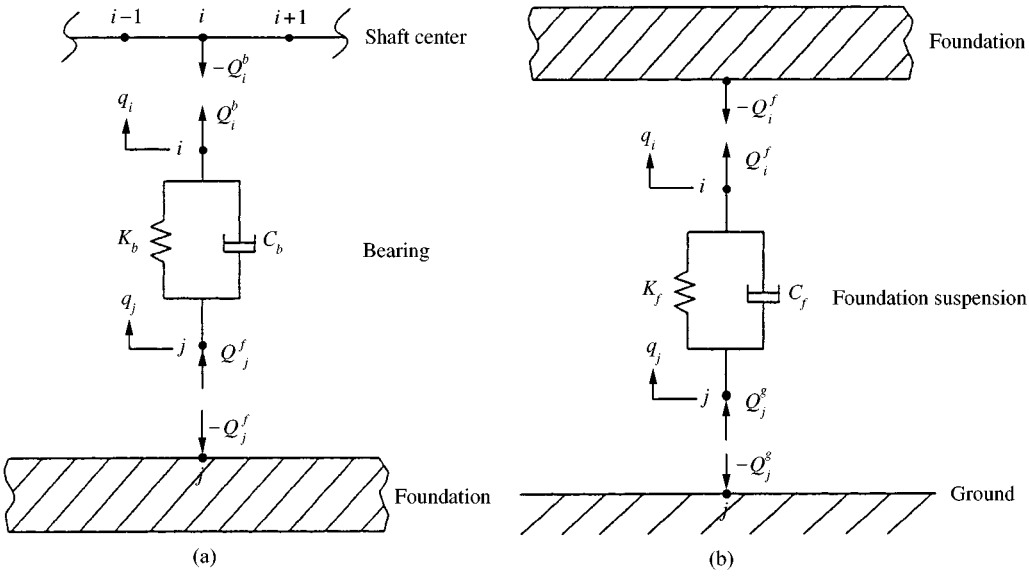

Figure. 3. The illustrations of force equilibrium of the bearing and suspension: (a) two-node model of linear bearing; (b) two-node model of linear suspension.

ANSYS is a common tool for finite element analyses, whose basic codes allow the rotating beam elements and the solid elements to model the shaft and the foundation respectively. For a rotating beam element, the gyroscopic effect can be taken into consideration. Also, the effects of rotary inertia, shear deformation, axial load and internal damping have been included. However, this package like most others does not set specific elements for modelling rotating disks, bearings and suspensions.

In ANSYS, MATRIX 27 is available for modelling rotating disk, bearing and suspensions. The geometry of this arbitrary element is undefined, but its mechanism can be specified by stiffness, damping, or mass matrix. The matrix is assumed to relate to two nodes, each with six d.o.f.s per node, translations in the nodal x, y, and z directions and rotations about the nodal x-, y-, and z axis. Other similar, but less general elements are the spring-damper element and the mass element.

3. DECOMPOSITION AND SYNTHESIS OF SUBSTRUCTURES

Three steps are required for the analysis. In step 1, both the finite element model of a rotor-bearing system and the foundation structure are constructed and meshed. In step 2, foundation matrices are introduced into the rotor-bearing equations via the formulation of interactive forces between component nodes. In step 3, standard codes are applied to calculate the characteristics of rotor-bearing–foundation systems. Modification in design procedures of the foundation of a rotor-bearing system can be suggested by the results of dynamic analyses.

Assembling equations (1)–(3) gives the motion equation of a rotor-bearing system as follows:

$$[M]\{\ddot{q}\} + [C]\{\dot{q}\} + [K]\{q\} = \Omega^2\{F_u\} + \{F_g\} + \{Q_b^f\} + \{Q_d^g\}. \tag{5}$$

Equation (5) can be separated into the sub-matrix form as

$$\begin{bmatrix} [M_{aa}] & [m_{ab}] \\ [m_{ba}] & [m_{bb}] \end{bmatrix} \begin{bmatrix} \{\ddot{q}_a\} \\ \{\ddot{q}_b\} \end{bmatrix} + \begin{bmatrix} [C_{aa}] & [c_{ab}] \\ [c_{ba}] & [c_{bb}] \end{bmatrix} \begin{bmatrix} \{\dot{q}_a\} \\ \{\dot{q}_b\} \end{bmatrix} + \begin{bmatrix} [K_{aa}] & [k_{ab}] \\ [k_{ba}] & [k_{bb}] \end{bmatrix} \begin{bmatrix} \{q_a\} \\ \{q_b\} \end{bmatrix}$$

$$= \begin{bmatrix} \{F_a\} \\ \{Q_b\} \end{bmatrix}, \tag{6}$$

where subscript "a" denotes all of the interior d.o.f. and free-end d.o.f. of the rotor-bearing system, and subscript "b" denotes the common d.o.f. of the bearing and the foundation.

Similarly, the motion equation of the foundation structure mounted on the suspension can be expressed as

$$\begin{bmatrix} [m'_{bb}] & [m'_{bc}] \\ [m'_{cb}] & [M'_{cc}] \end{bmatrix} \begin{bmatrix} \{\ddot{q}_b\} \\ \{\ddot{q}_c\} \end{bmatrix} + \begin{bmatrix} [c'_{bb}] & [c'_{bc}] \\ [c'_{cb}] & [C'_{cc}] \end{bmatrix} \begin{bmatrix} \{\dot{q}_b\} \\ \{\dot{q}_c\} \end{bmatrix} + \begin{bmatrix} [k'_{bb}] & [k'_{bc}] \\ [k'_{cb}] & [K'_{cc}] \end{bmatrix} \begin{bmatrix} \{q_b\} \\ \{q_c\} \end{bmatrix}$$

$$= \begin{bmatrix} -\{Q_b\} \\ \{F_c\} \end{bmatrix}, \tag{7}$$

where subscript "c" denotes the interior d.o.f. and free-surface d.o.f. of the foundation. The motion equations of foundation are modelled by proper elements, such as beam, plate, shell or solid elements, which are provided by ANSYS coding. Asembling equations (6) and (7) gives

$$\begin{bmatrix} [M_{aa}] & [m_{ab}] & [0] \\ [m_{ba}] & [m_{bb} + m'_{bb}] & [m'_{bc}] \\ [0] & [m'_{cb}] & [M'_{cc}] \end{bmatrix} \begin{bmatrix} \{\ddot{q}_a\} \\ \{\ddot{q}_b\} \\ \{\ddot{q}_c\} \end{bmatrix} + \begin{bmatrix} [C_{aa}] & [c_{ab}] & [0] \\ [c_{ba}] & [c_{bb} + c'_{bb}] & [c'_{bc}] \\ [0] & [c'_{cb}] & [C'_{cc}] \end{bmatrix} \begin{bmatrix} \{\dot{q}_a\} \\ \{\dot{q}_b\} \\ \{\dot{q}_c\} \end{bmatrix}$$

$$+ \begin{bmatrix} [K_{aa}] & [k_{ab}] & [0] \\ [k_{ba}] & [k_{bb} + k'_{bb}] & [k'_{bc}] \\ [0] & [k'_{cb}] & [K'_{cc}] \end{bmatrix} \begin{bmatrix} \{q_a\} \\ \{q_b\} \\ \{q_c\} \end{bmatrix} = \begin{bmatrix} \{F_a\} \\ 0 \\ \{F_c\} \end{bmatrix}, \tag{8}$$

where $\{F^a\}$ and $\{F^c\}$ are vectors of external loads applied at the rotor and at the foundation respectively. Solver codes of ANSYS can be applied to determine natural frequencies, mode shapes, critical speeds, stability thresholds, unbalance responses of rotor-bearing–foundation models for the analysis of foundation effects.

4. MODE TRANSITIONS DUE TO INFLUENCES OF LUMPED-MASS FOUNDATIONS

The Jeffcott rotor shown in Figure 4, is the simplest model of a rotor-bearing–foundation system. It is supported by discrete foundations at both ends. The details of lumped-mass foundation modelling are shown in Appendix B. This model has physical parameters as listed in Table 1 and is validated through four cases of different stiffness coefficients of suspension K_f: 10^3, 10^5, 10^7 and 10^9 N/m.

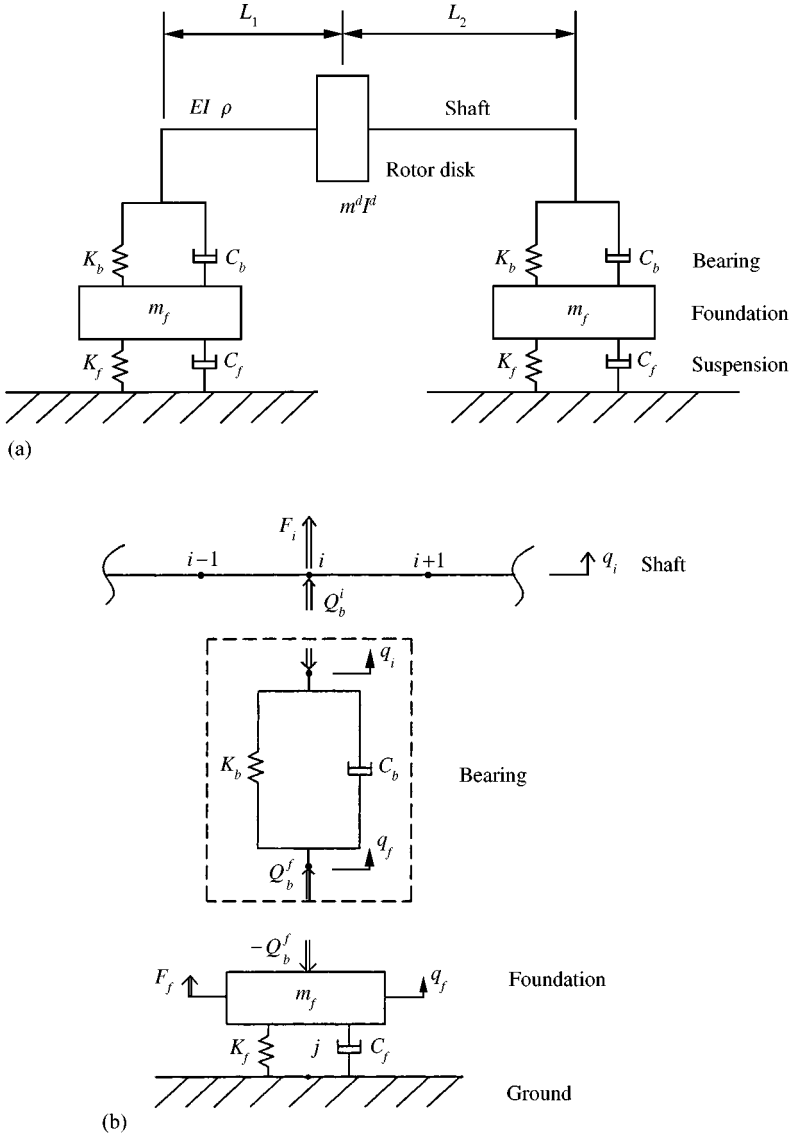

Figure. 4. The model of rotor-bearing system mounted on lumped mass foundation: (a) system; (b) two-node model of a lumped-type foundation.

TABLE 1

Physical parameters of the model in Figure 4

Bearings	$K_{xx} = K_{yy} = 10^9$ or 10^5 N/m, others = 0
Disk	$m^d = 0{\cdot}4127$ kg, $I^d = 1{\cdot}6076 \times 10^{-4}$ kg m^2, $J^d = 3{\cdot}0187 \times 10^{-4}$ kg m^2
Shaft	$E = 2 \times 10^{11}$ N/m^2, $I = 4{\cdot}0489 \times 10^{-10}$ m^4, $\rho = 7850$ kg/m^3, $L_1 = 0{\cdot}2$ m, $L_2 = 0{\cdot}3$ m
Foundations	$m_f = 0{\cdot}01\ m_r$, $1\ m_r$, $10\ m_r$, $100\ m_r$, ($m_r = 0{\cdot}6926$ kg)
Suspensions	$K_{xx} = K_{yy} = 10^9$ or 10^5 N/m, others = 0

From modal analysis of the equations of the overall system, natural frequencies of the first nine modes, $\omega_1, \omega_2, \ldots, \omega_9$ in ascending order, can be obtained versus m_f/m_r as shown in Figure 5. These results show that the natural frequencies of each mode decrease as the foundation mass increases. In Figure 5, the variation of natural frequencies can be separated into three parts. When the mass ratio of foundation m_f/m_r is either sufficiently large or small, the natural frequencies change slightly as m_f/m_r varies. While the foundation mass has a medium value, the intensive transition of natural frequencies occurs as the value of m_f varies a little.

After transition, the shape of a high order flexural mode of the rotor is influenced by large m_f and is thus transformed into a lower order flexural mode. As shown in Figure 5(c), the value of m_f/m_r increases from 0·1 to 10, the natural frequencies of ω_3 to ω_7 decrease to the frequencies of ω_1 to ω_5, and the mode shapes are transferred from ω_n to ω_{n-2} at the same time.

It should be noted that the transition of resonant modes occurs in spite of the stiffness coefficients of suspension K_f. Yet, the only difference is in the range of m_f/m_r when the transition actually occurs. The transition occurs at large values of m_f/m_r when suspensions are stiff or when K_f is sufficiently large.

The shadow zone is used to indicate the allowable range of operating speed. The ranges between any two adjacent modes are available for operation. When the suspension is soft, the rotor is accelerated to pass through the first several rigid-body modes rapidly and is rotated at a speed below to the critical speeds of flexural modes of the rotor. Thus, the motion of foundation mass has no limit.

Conversely, when the suspension is hard, for example $K_f = 10^7$ to 10^9 N/m, the range of m_f where the resonant transition occurs is not available. For example, when $K_f = 10^7$ N/m, a range of m_f/m_r from 1 to 40 must be avoided, and a value of m_f/m_r greater than 100 as $K_f = 10^9$ N/m is also not recommened.

The stiffness coefficients of most bearings, for instance, the angular contact ball bearings, the tapered roller bearings, the hybrid oil-film bearings and the big-size hydrodynamic journal bearings, are between 10^8 and 10^9 N/m.

However, the stiffness coefficients of small-size oil-film bearings or hydrostatic air bearings have values from 10^6 to 10^7 N/m, or smaller values. Thus, the analyses for small coefficients of bearing stiffness have also been studied.

Similar to the phenomena of hard bearings shown in Figure 5, the natural frequencies of the system (Figure 4) mounted on soft bearings (for example, $K_b = 10^5$ N/m) decrease as the foundation mass increases, and the results are

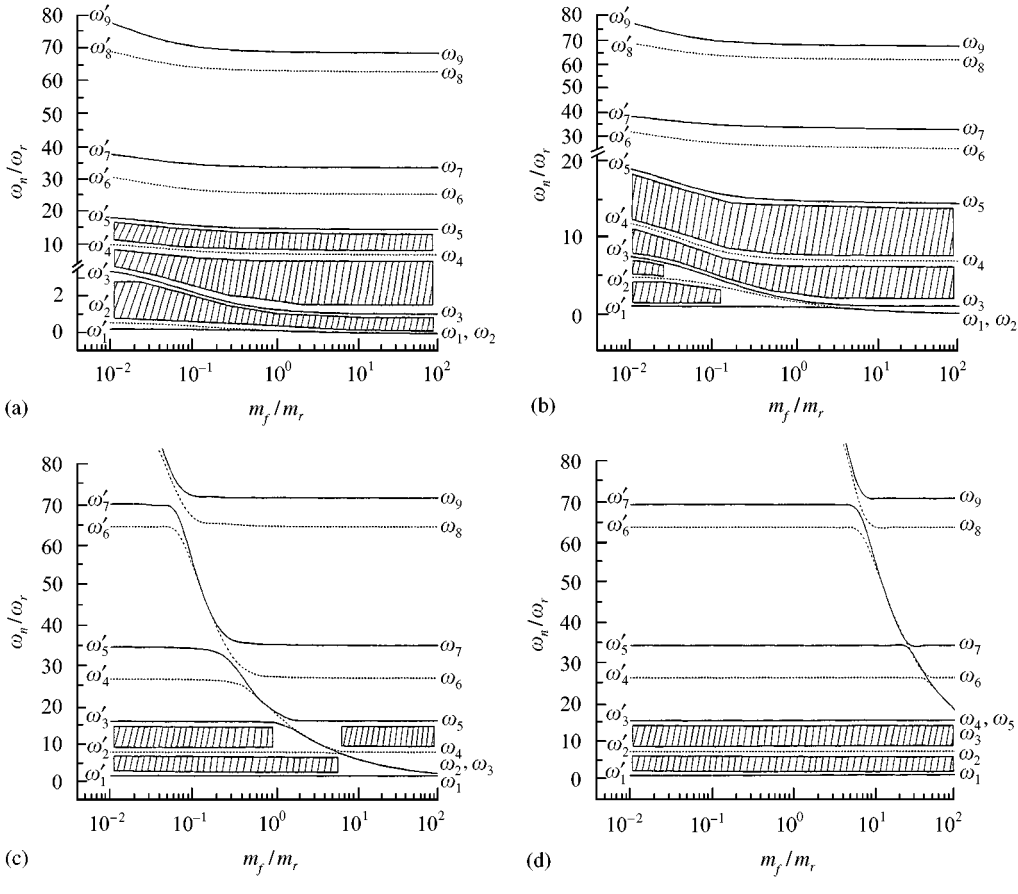

Figure. 5. The natural frequencies versus the foundation mass and $K_b = 10^9$ N/m: (a) $K_f = 10^3$ N/m; (b) $K_f = 10^5$ N/m; (c) $K_f = 10^7$ N/m; (d) $K_f = 10^9$ N/m.

shown in Figure 6. However, the difference between them is that the soft bearings have more modes than the hard bearings within the same speed range. Obviously, the safe range of operation for a rotor mounted on soft bearings is smaller than that of the one mounted on hard bearings.

Applying the similar analysis to the situation when $K_b = 10^9$ and 10^5 N/m, one can get the natural frequencies of mode versus foundation stiffness as shown in Figures 7 and 8. In both figures, the values of m_f/m_r are chosen as 100, 10, 1, 0·01.

The natural frequencies of each mode increase as K_f increases. When K_f is either very large or very small, the natural frequencies of mode increase smoothly. However, as long as the values of K_f range are medium, violent transitions of the natural frequencies occur as K_f varies lightly.

The ranges between two adjacent modes are larger and the number of modes is lower within a speed range as m_f gets smaller. Also, the transition of natural frequencies occurs at a smaller value of K_f and the range of transition is narrower. Thus, the smaller the foundation mass m_f is, the larger the range of available K_f is.

As shown in Figure 7, when the foundation mass m_f is larger, the transition occurs at larger values of bearing stiffness. After transition, all the resonant modes

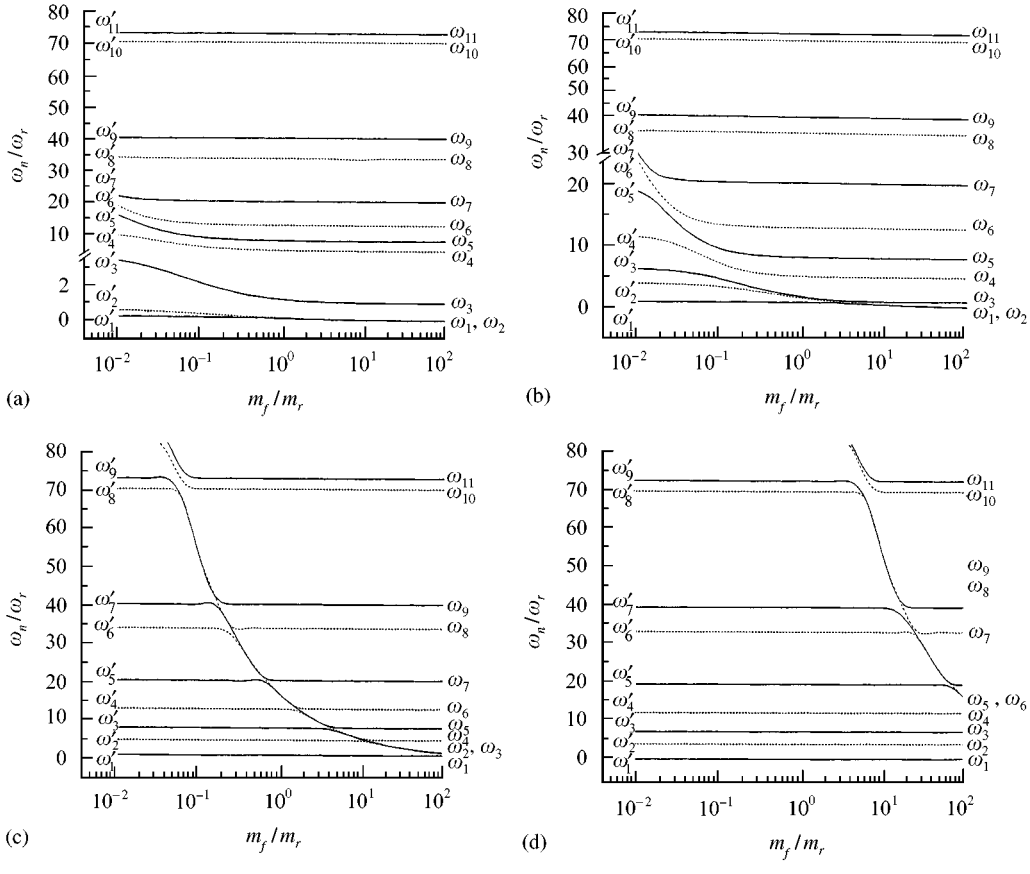

Figure. 6. The natural frequencies versus the foundation mass and $K_b = 10^9$ N/m: (a) $K_f = 10^3$ N/m; (b) $K_f = 10^5$ N/m; (c) $K_f = 10^7$ N/m; (d) $K_f = 10^9$ N/m.

veer to the modes of the rotor-bearing system that is simply supported by rigid foundation.

In Figure 8, before the transitions, the first and second modes of the system are coupled by the rigid-body motions of foundation and of rotor respectively. After the transitions, the first and second modes veer to the coupled flexural mode of the rotor and a rigid-body motion mode of the rotor. All flexural modes of the system are coupled by a flexural mode of the rotor and a rigid-body motion mode of the foundation before the transition, and they veer to flexural modes of rotor after the transitions.

Figure 9 illustrates the transitions as mentioned above for the first three modes of a one-disk rotor-bearing–foundation model, $K_f/K_b = 10^{-4}$ (before the transition) and $K_f/K_b = 10^7$ (after the transition), respectively. The bearing stiffness of this model is $K_b = 10^9$ N/m. In this figure, the displacements of the rotor at both ends are denoted by A_{r1} and A_{r2} respectively, the center displacement of the disk is denoted by A_{r3}, and the displacements of foundation at both ends are denoted by

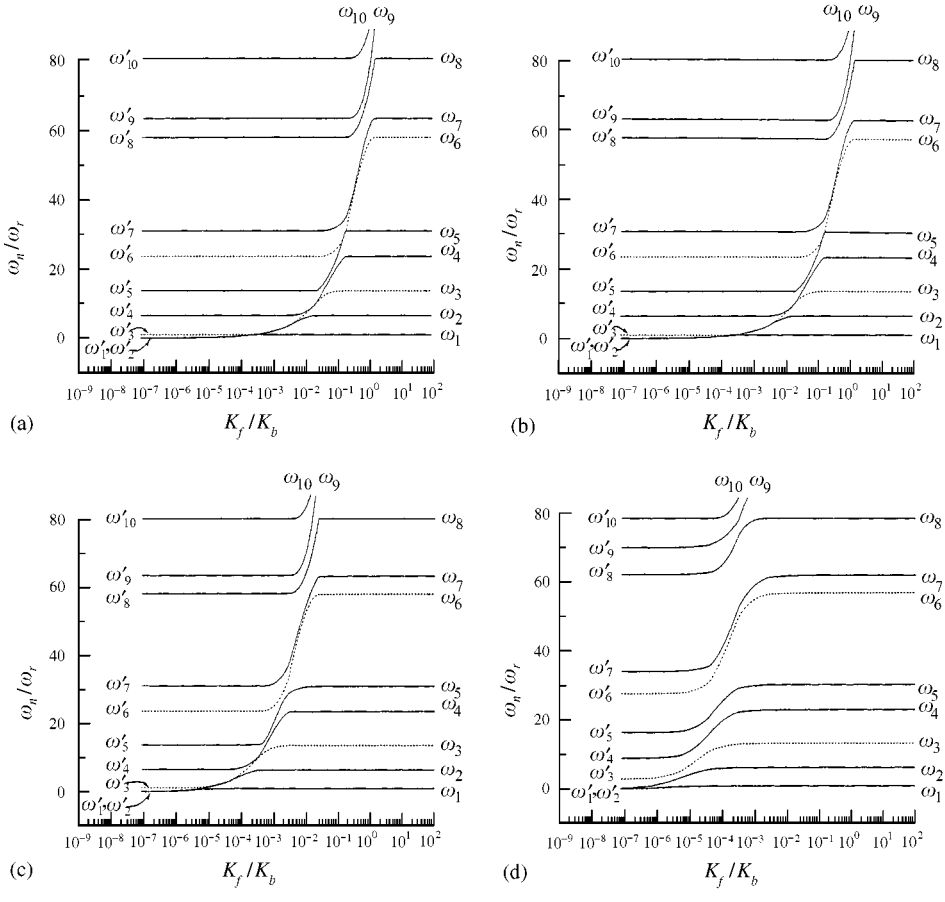

Figure. 7. The natural frequencies versus the suspension stiffness and $K_b = 10^9$ N/m: (a) $m_f/m_r = 100$, (b) $m_f/m_r = 10$, (c) $m_f/m_r = 1$, (d) $m_f/m_r = 0{\cdot}01$.

A_{f1} and A_{f2} respectively. The amplitude ratios of the displacements related to $A_{r1} = 1$ for mode shapes are listed in Table 2.

5. COUPLING EFFECTS OF FLEXIBLE CONTINUOUS FOUNDATIONS

For the analysis of cross-coupling effects between two bearing support points, a Jeffcott rotor mounted on a beam-type foundation as shown in Figure 10 is taken into consideration. The finite element models of the foundation and the rotor are combined by bearings which are modelled by a two-node element provided by the ANSYS library. Two cases are determined: (1) finite element matrices by ignoring the cross-coupling term of the foundation and (2) complete finite element matrices of the foundation.

The physical parameters of this rotor-bearing–foundation system are listed in Table 3. The beam is supported by suspensions at both ends and both suspension points are located just below the two bearings. It is assumed that the bearing and

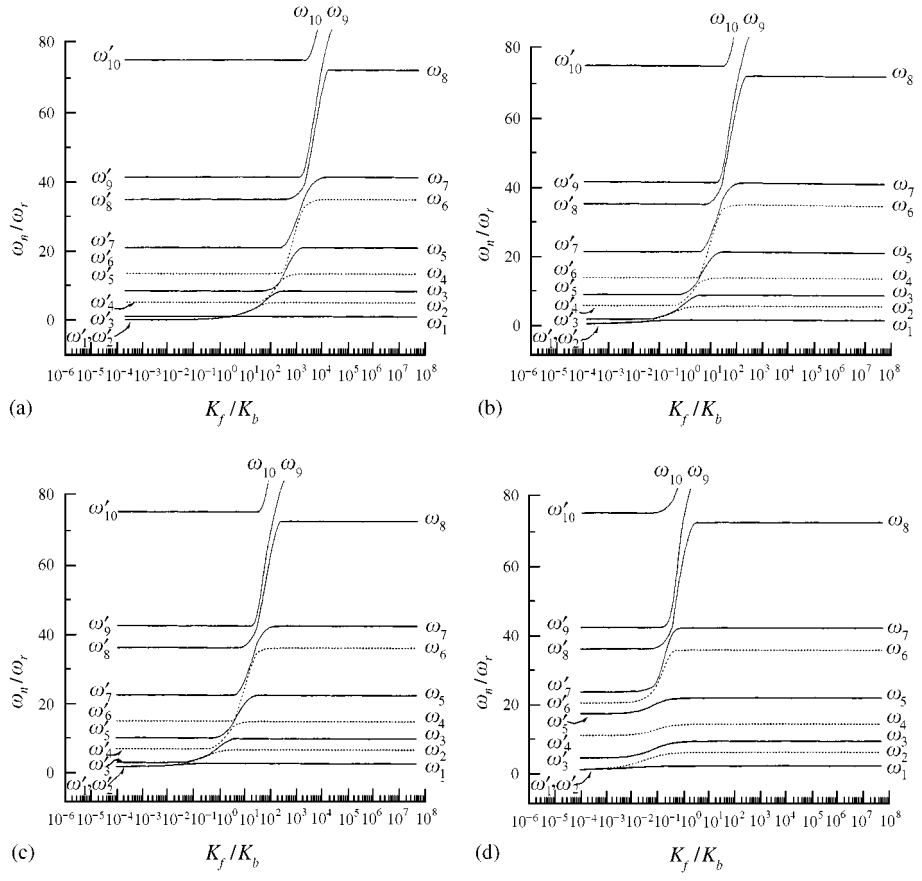

Figure. 8. The natural frequencies versus the suspension stiffness and $K_b = 10^5$ N/m: (a) $m_f/m_r = 100$, (b) $m_f/m_r = 10$, (c) $m_f/m_r = 1$, (d) $m_f/m_r = 0{\cdot}01$.

foundation are isotropic and symmetric around the shaft, and stiffness coefficients are identical for both the vertical and horizontal directions.

The unbalance responses are shown in Figure 11 for the spin speed from 0 to 2000 Hz, where the ordinate is amplitude, logarithm to base 10, and the unit is meter. The coupling effects of supported points of bearings is illustrated by the solid lines, which is induced by the foundation flexibility. The dashed lines represent the results without coupling effect by removing cross-coupling elements of stiffness matrix.

When both bearing and suspension are soft, as shown in Figure 12, the cross-coupling effect degrades the natural frequencies of resonant modes. If K_b is large and K_f is small, the cross-coupling effect increases the number of modes within an identical frequency range. In contrast, when both bearing and suspension are hard, the cross-coupling effect is nil, as shown in Figure 13.

Also when only the stiffness of the foundation is sufficiently large, the cross-coupling is ineffective, as shown in both Figures 11(a) and 12(a). For a 0·2 m thick foundation, the analytical results of the foundation with cross-coupling or ignoring element of cross-coupling are identical, while for the 0·02 or 0·002 m thick foundations, the results are distinct.

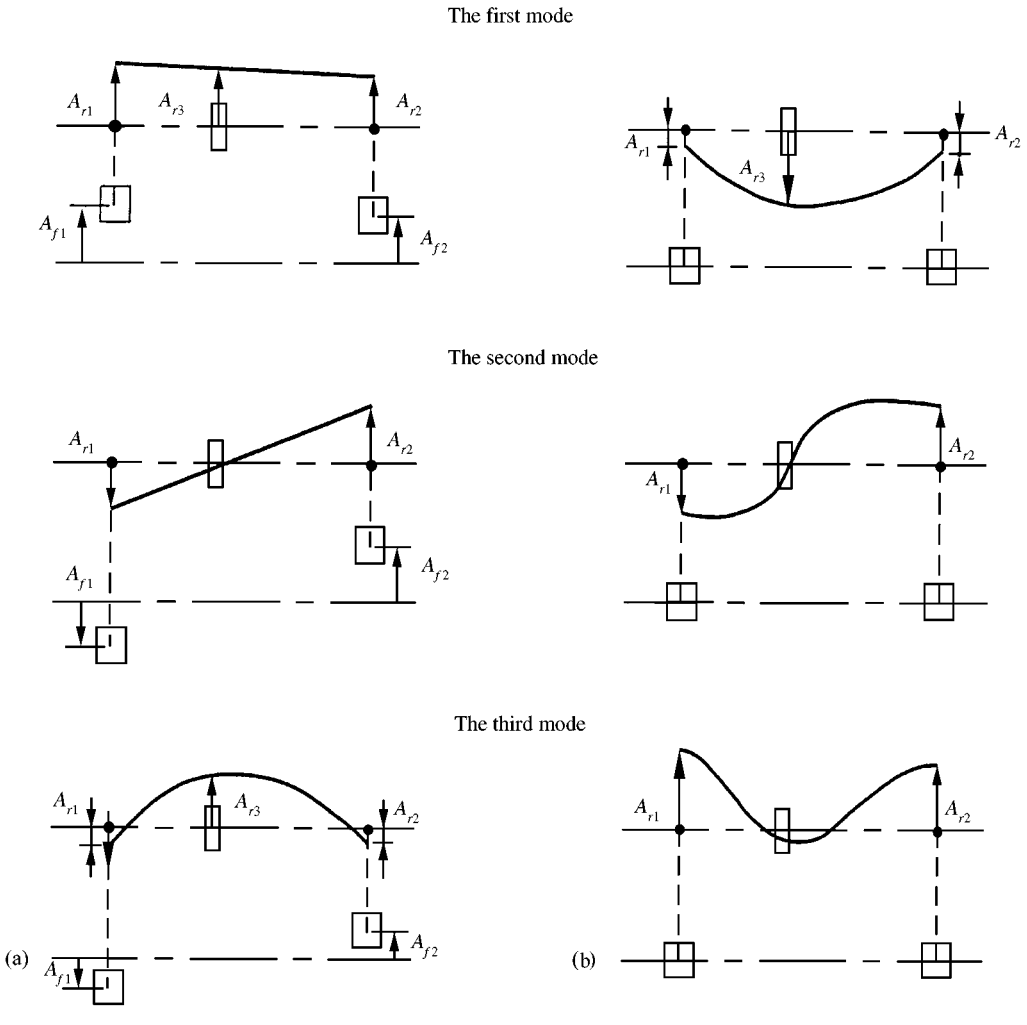

Figure. 9. The first three modes for two suspension stiffness. (a) $K_f/K_b = 10^{-4}$; (b) $K_f/K_b = 10^7$.

TABLE 2

Mode shapes of both cases

K_f/K_b	Elements of mode vector	A_{r1}	A_{r2}	A_{r3}	A_{f1}	A_{f2}
10^{-4}	1st mode	1	0·7549	0·9021	1	0·7551
	2nd mode	−1	1·3237	− 0·0701	0·9996	1·3233
	3rd mode	−1	− 0·7519	4·2918	− 2·0457	1·5394
10^7	1st mode	−1	− 0·7546	5·7170	0	0
	2nd mode	−1	1·3821	0·1771	0	0
	3rd mode	1	0·7099	− 0·0829	0	0

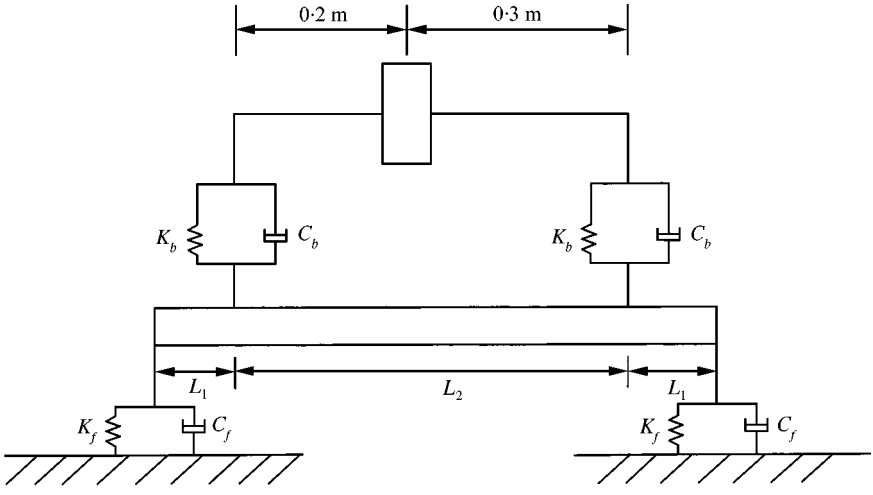

Figure. 10. Jeffcott rotor mounted on a beam-type foundation.

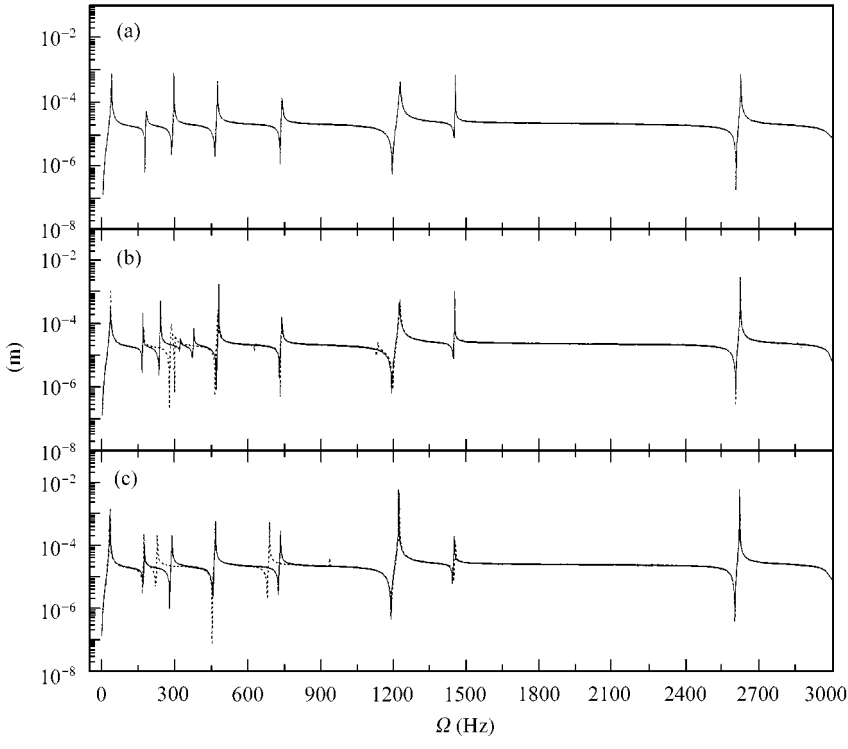

Figure. 11. Harmonic responses for $K_b = K_f = 10^5$ N/m, and $D =$ (a) 0·2 m, (b) 0·02 m, (c) 0·002 m.

6. INFLUENCES ON CAMPBELL DIAGRAM

The first eight resonant frequencies versus the spin speed of a rotor-bearing–foundation system are shown in Figure 4. Table 1 is determined, whose Campbell diagrams for various mass ratios (m_f/m_r) are shown in Figure 14. Due to

TABLE 3

Physical parameters of the model in Figure 10

Bearings	$K_{xx} = K_{yy} = 10^9$ or 10^5 N/m, others = 0
Foundation	$E = 2 \times 10^{11}$ N/m^2, $I_x = I_y = I = 0{\cdot}04909D^4$ from 10^{-10}–10^{-6} m^4, $\rho = 7850$ kg/m^3, $L_1 = 0$, $L_2 = 0{\cdot}5$ m
Disk	$m^d = 0{\cdot}4127$ kg, $I^d = 1{\cdot}6076 \times 10^{-4}$ kg m^2, $J^d = 3{\cdot}0187 \times 10^{-4}$ kg m^2
Shaft	$E = 2 \times 10^{11}$ Pa, $I = 4{\cdot}0489 \times 10^{-10}$ m^4, $\rho = 7850$ kg/m^3
Suspensions	$K_{xx} = K_{yy} = 10^9$ or 10^5 N/m, others = 0

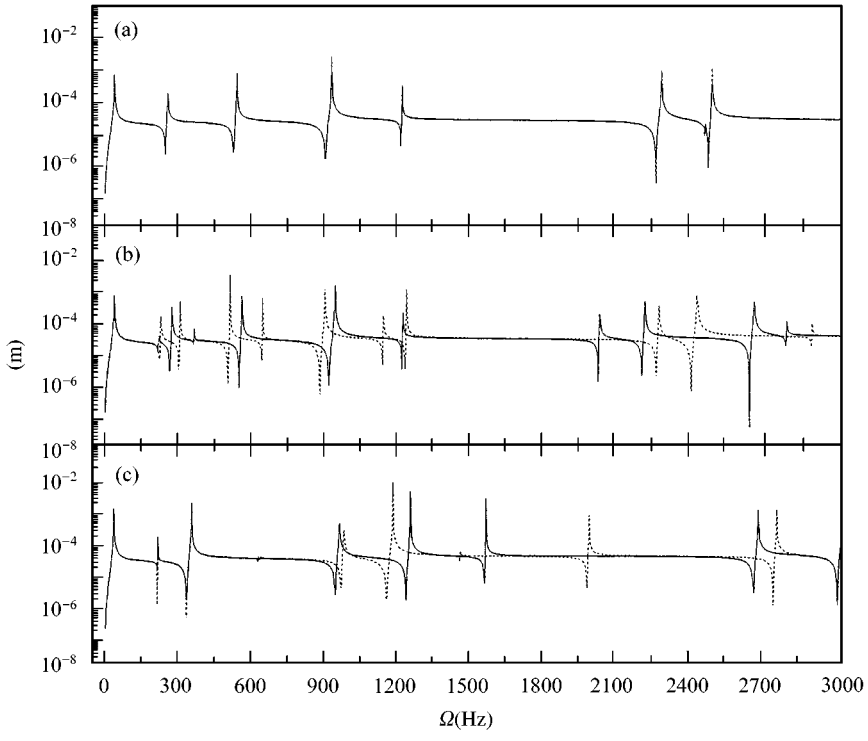

Figure. 12. Harmonic responses for $K_b = 10^9$ N/m, $K_f = 10^5$ N/m, and $D =$ (a) 0·2 m, (b) 0·02 m, (c) 0·002 m.

the gyroscopic effects of rotating shafts and disks, each mode has both forward and backward whirls. In this figure, *nF* and *nB* denote the *n*th order modes of forward and backward whirls respectively, and *nM* denotes the *n*th mode of independent motion of the foundation. The natural frequencies of the foundation mode remain constant while speed varies, since the gyroscopic effect is nil.

When the stiffness coefficients of bearing and suspension are all small, for instance, where both K_b and K_f are 10^5 N/m, coupled motions of foundation and rotor coexist in a single mode. When K_b and K_f are large, for instance, $K_b = K_f = 10^9$ N/m, only one motion of rotor or foundation exists in one mode.

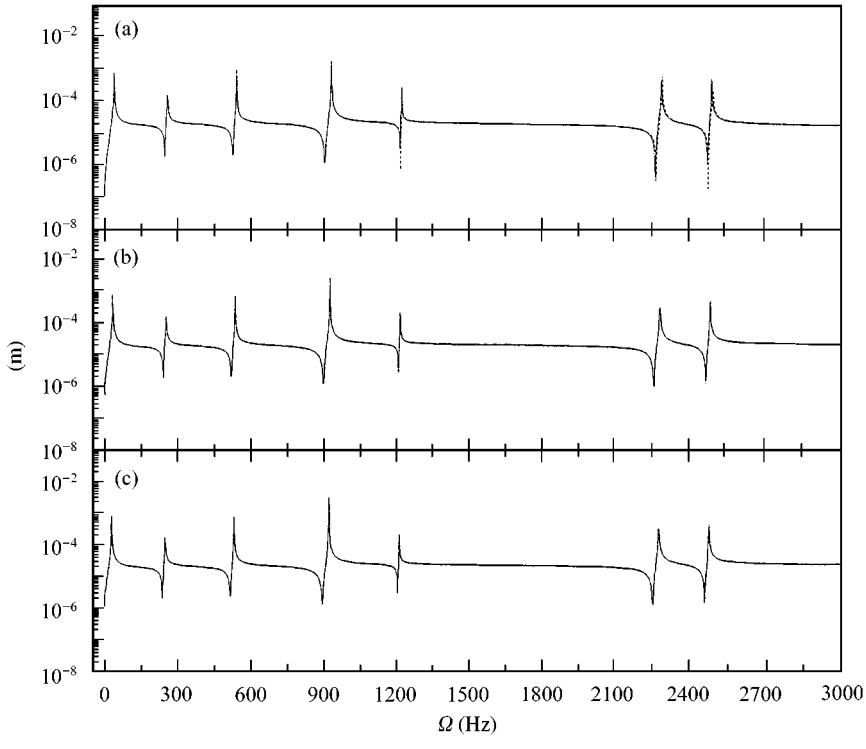

Figure. 13. Harmonic responses for $K_b = K_f = 10^9$ N/m, and $D =$ (a) 0·2 m, (b) 0·02 m, (c) 0·002 m.

For $m_f/m_r = 100$, the first mode of foundation can be below 1100 Hz. While the value of m_f is small (for example, $m_f/m_r = 1$ or 0·01), the frequency of fundamental mode of foundation has a higher value.

For the same stiffness coefficient, the value of m_f is less and the natural frequency of identical mode is larger at zero speed. When spin speed increases, the frequencies of forward modes rise rapidly and the frequencies of backward modes also degrade rapidly.

For the same value of m_f/m_r, the number of modes in a frequency range decrease as the values of K_b and K_f increase. For $K_b = K_f = 10^5$ N/m, the bifurcation of the even-order modes is greater and the bifurcation of the odd-order modes is smaller. For $K_b = K_f = 10^9$ N/m, the bifurcation of the first and second modes are smaller; in contrast, the bifurcation of the other modes has a similar degree.

7. EFFECTS ON CRITICAL SPEEDS AND HARMONIC RESPONSES

The same rotor-bearing–foundation system as shown in Figure 10 has $K_b = 10^9$ N/m, $K_f = 10^5$ N/m, shaft radius 0·02 m and varying moment of area from 10^{-10} to 10^{-6} m^4 of beam-type foundation. The harmonic responses due to rotating unbalance are determined and are shown in Figure 15. From these results,

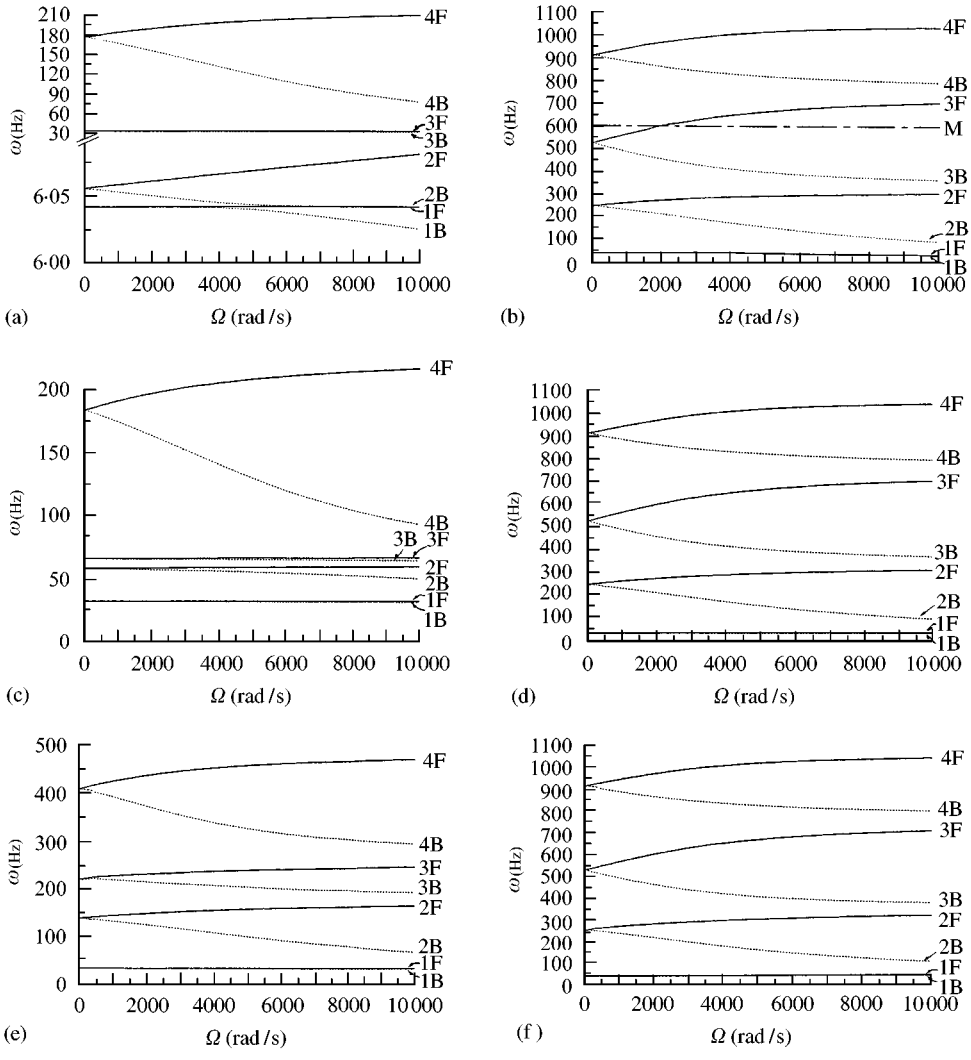

Figure. 14. Campbell diagrams (a)–(c): $K_f = K_b = 10^5$ N/m; (d)–(f): $K_f = K_b = 10^9$ N/m: ——, forward whirl (F); - - - - -, backward whirl (B); — — —, mode of foundation (M) ((a, d) $m_f/m_r = 100$; (b, c) $m_f/m_r = 1$; (c, f) $m_f/m_r = 0{\cdot}01$).

the variation of critical speeds versus moment of area I is presented in Figure 16. When moment of area I exceeds 10^{-8} m^4, mass and stiffness of foundation also increase as I increases, and thus the increase in I reduces the critical speed slightly. When I is smaller than 10^{-8} m^4, the critical speed rises conspiciously as I increases due to the dominant effect of the increase in stiffness.

In Figure 16, 1 Hz below the first mode, 100 Hz in a frequency range between the second and the third modes, and 200 Hz beyond the third mode range are selected. These are considered in the determination of the harmonic responses for the disk center of the rotor. The analytical results are shown in Figure 17.

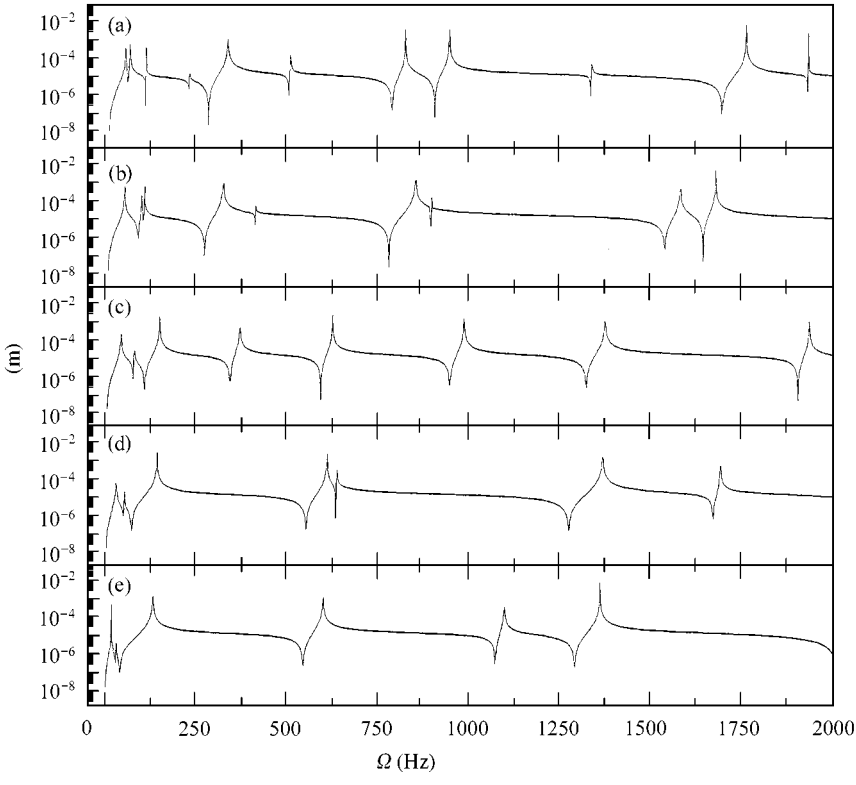

Figure. 15. Harmonic responses of rotor-bearing–foundation system for $K_b = 10^9$ N/m, $K_f = 10^5$ N/m in Figure 10: (a) $I = 10^{-10}$ m^4; (b) $I = 10^{-9}$ m^4; (c) $I = 10^{-8}$ m^4; (d) $I = 10^{-7}$ m^4; (e) $I = 10^{-6}$ m^4.

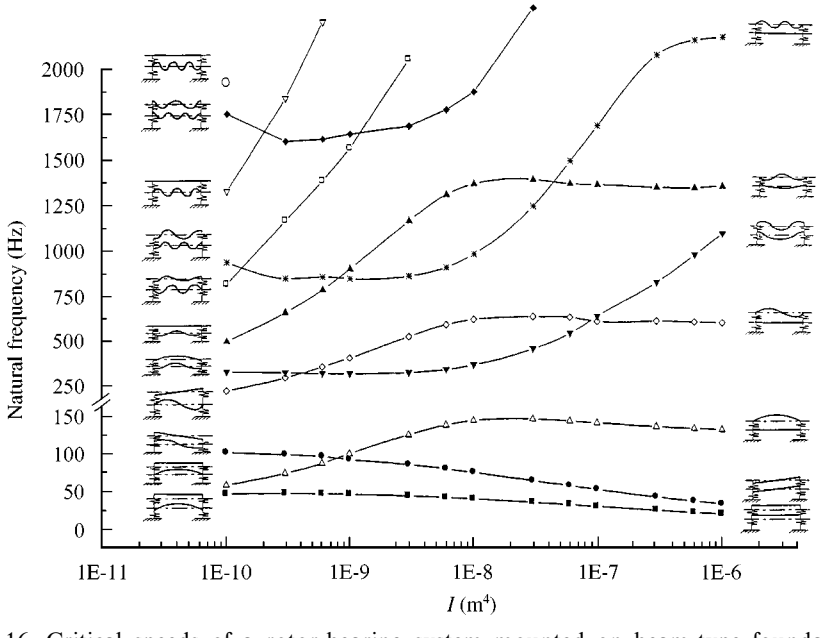

Figure. 16. Critical speeds of a rotor-bearing system mounted on beam-type foundation with $K_b = 10^9$ N/m, $K_f = 10^5$ N/m.

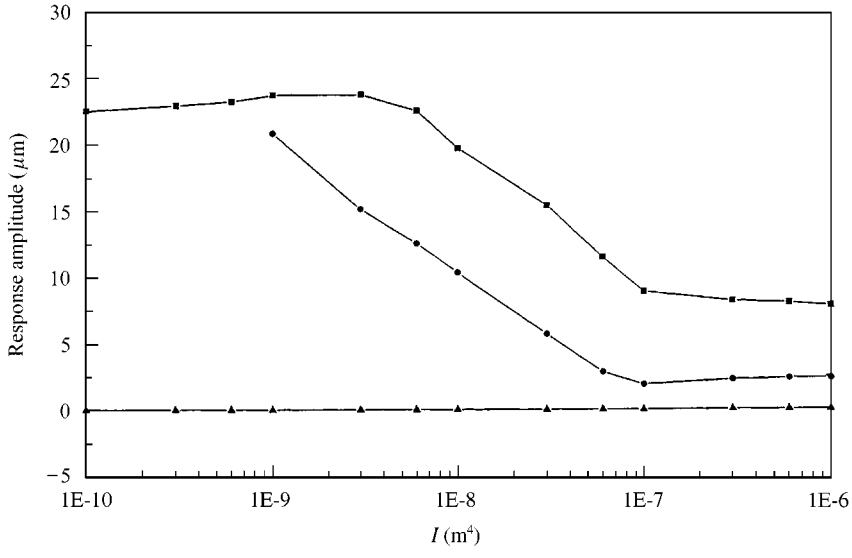

Figure. 17. Harmonic responses at 1, 100, 200 Hz with $K_b = 10^9$ N/m, $K_f = 10^5$ N/m: —■—, spin speed 200 Hz; —●—, spin speed 100 Hz; —▲—, spin speed 1 Hz.

The range of spin speed of the rotor can be designed according to the results of Figure 16; furthermore, Figure 17 is useful for the design of moment of area I of the foundation. When the moment of area I of the foundation is greater than 10^{-7} m^4, the harmonic responses cannot be suppressed by increasing I. However, the foundation mass increases as moment of area I increases. This causes the critical speeds of modes to decrease and the range of operating speed to narrow. Thus, from this example, the optimal value of I determined is 10^{-7} m^4.

The analytical results of critical speeds and the harmonic responses at 1, 100, 200, 400 Hz for hard foundation suspensions (for example $K_f = 10^9$ N/m) and hard bearings (for example, $K_b = 10^9$ N/m) are shown in Figures 18 and 19 respectively. For $I = 10^{-10}$ m^4, the second, fifth, and seventh modes are referred to as the decoupled modes of rotor. Also the critical speeds do not vary with moment of area I since the foundation does not deform at these three modes. The fourth, sixth, eighth, and ninth modes are referred to as the decoupled modes of foundation, and the rotor is stationary without deformation. In addition, the first and third modes are the coupled modes of rotor and foundation. Consequently, the critical speeds of foundation modes increase as moment of area I increases.

Figure 19 represents the responses versus moment of area I at four spin speeds. Since stiffness coefficients K_f and K_b are sufficiently large, all the responses remain constant unless the resonance occurs as shown.

For foundation design, the choice of an appropriate moment of area I is beneficial for a wider range of two adjustment critical speeds. As shown in Figure 18, it is better to utilize a value of I which is greater than 10^{-18} m^4 as the operating speed is near 100 Hz. When the operating speed is near 200 Hz, the value of I should preferably be less than 5×10^{-9} m^4 or greater than 5×10^{-8} m^4 and when

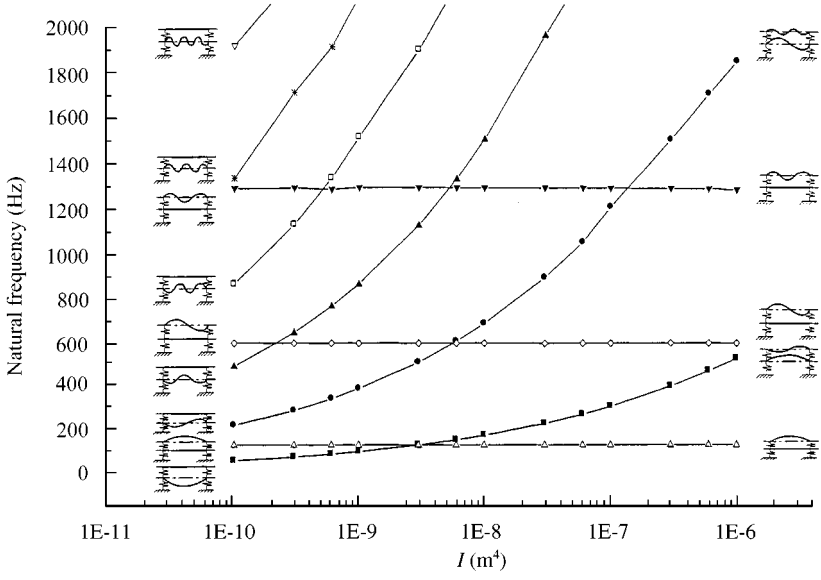

Figure. 18. Critical speeds of a rotor-bearing system mounted on beam-type foundation with $K_b = K_f = 10^9$ N/m.

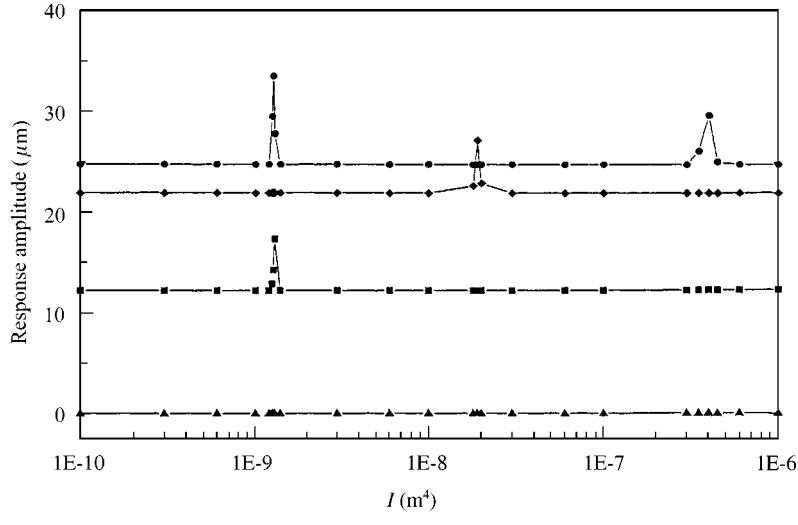

Figure. 19. Harmonic responses for rotor-bearing system mounted on beam-type foundation with $K_b = K_f = 10^9$ N/m: —▲—, spin speed 1 Hz; —◆—, spin speed 200 Hz; —■—, spin speed 100 Hz; —●—, spin speed 400 Hz.

the operating speed is near 400 Hz, the optimal range of I is between 2×10^{-9} and 10^{-7} m^4.

Figure 20 reveals the critical speeds versus moment of area I of the foundation, when both the stiffness coefficients of bearing and suspension are soft. In this figure, $K_f = 10^5$ N/m $= K_b$ is assumed and mode shapes are illustrated on both ends of each curve. The lowest three modes are coupled by rigid-body motions of rotor and

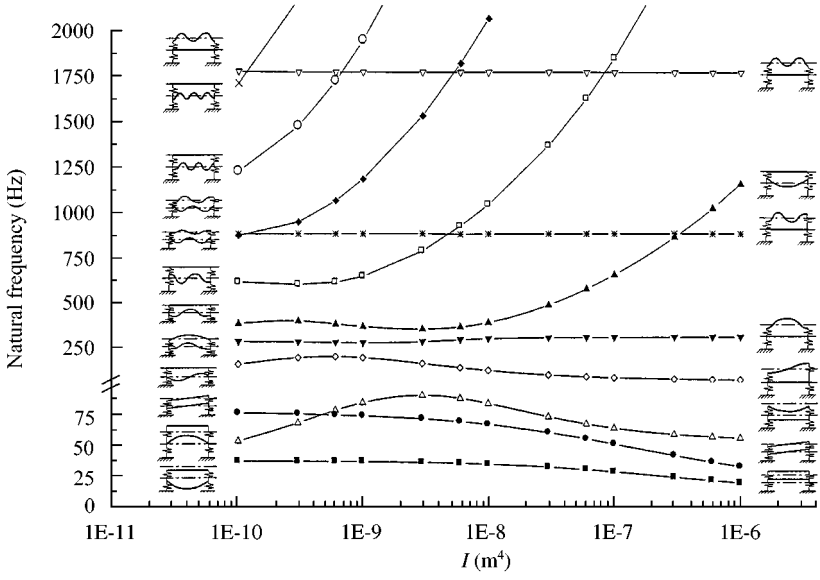

Figure. 20. Critical speeds of a rotor-bearing system mounted on beam-type foundation with $K_b = K_f = 10^5$ N/m.

foundation. Specifically, the second mode processes flexural deformation of foundation as I is small, and the natural frequency of this mode increases as I increases. However, when I is large and the mode shape is a coupled rigid-body motion, the natural frequency of this mode decreases as I increases.

The appropriate range of operating speeds is less than 25 Hz, or between 50 and 70 Hz, and the value of I is from 5×10^{-10} to 2×10^{-8} m^4. For a high-speed operation, a range between 100 and 200 Hz is acceptable disregarding the value of I.

8. CASE STUDIES OF FOUNDATION DESIGN

Two rotor-bearing–foundation kits as shown in Figure 21 have been studied through the modal analysis and the steady state analysis. A shaft with two or three detachable disks is mounted on two deep-groove ball bearings. These rotor-bearing systems are supported by a plate-type foundation. The overall structures are then supported by a soft suspension whose stiffness coefficient is estimated as 8×10^5 N/m. Physical and material parameters of both kits are listed in Table 4.

Disks, bearings, and suspensions of both kits are modelled by a two-node element as described by equations (2)–(4). The shaft is modelled by a beam element which includes the gyroscopic effect, the transversal inertia, the rotary inertia, and the shear deformation. The foundation is modelled by solid elements and the motor is modelled by a lumped mass element.

In modal testing, the rotor and foundation are excited by an impacted hammer and the responses are measured by using displacement sensors and accelerometers. The transfer functions of the rotor-bearing–foundation system are determined by

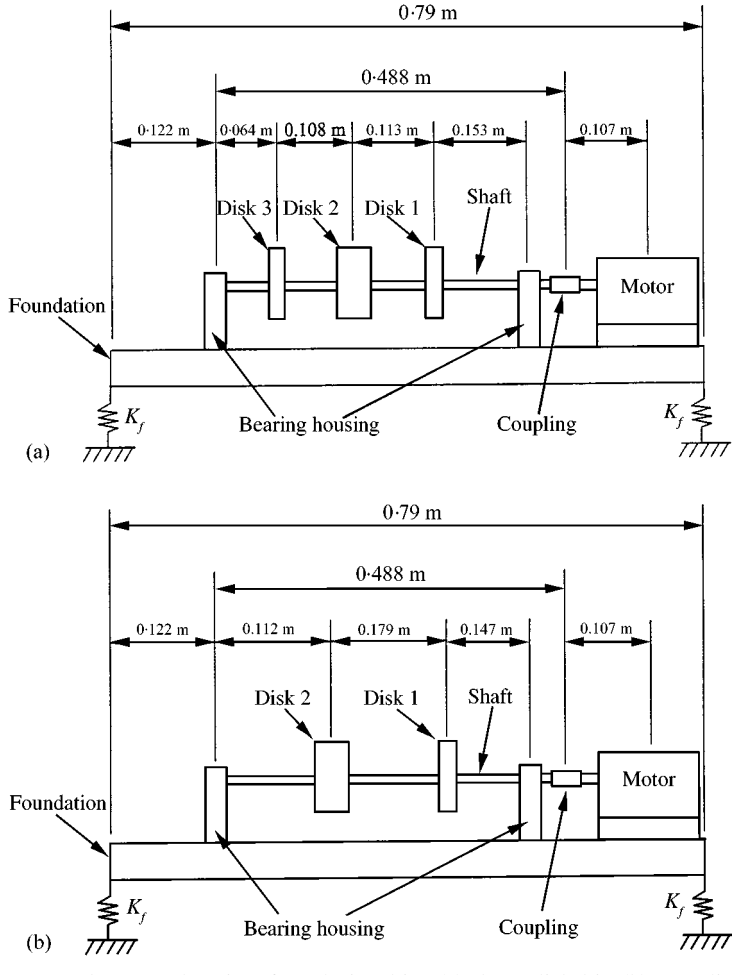

Figure. 21. The rotor-bearing–foundation kits: (a) three-disk kit; (b) two-disk kit.

TABLE 4

Physical parameters of the rotor-bearing–foundation model in Figure 21

Bearings	$K_{xx} = K_{yy} = K_b = 0 \sim 10^9$ N/m, others = 0
Foundations	$E = 7{\cdot}0 \times 10^{10}$ N/m^2, $\rho = 2710$ kg/m^3, $K_f = 8 \times 10^5$ N/m
	length = 0·79 m, width = 0·154 m, thickness = 0·025 m
Disk 1	$m^d = 0{\cdot}334$ kg, $I^d = 1{\cdot}36 \times 10^{-4}$ kg m^2, $J^d = 2{\cdot}688 \times 10^{-4}$ kg m^2
Disk 2	$m^d = 0{\cdot}782$ kg, $I^d = 4{\cdot}31 \times 10^{-4}$ kg m^2, $J^d = 7{\cdot}02 \times 10^{-4}$ kg m^2
Disk 3	$m^d = 0{\cdot}412$ kg, $I^d = 1{\cdot}525 \times 10^{-4}$ kg m^2, $J^d = 2{\cdot}983 \times 10^{-4}$ kg m^2
Shaft	$E = 2 \times 10^{11}$ N/m^2, $I = 4{\cdot}909 \times 10^{-10}$ m^4, $\rho = 7850$ kg/m^3
Motor	$m = 4{\cdot}39$ kg, $I_{xx} = 1{\cdot}389 \times 10^{-2}$ kg m^2, $I_{yy} = 1{\cdot}194 \times 10^{-2}$ kg m^2,
	$I_{zz} = 8{\cdot}809 \times 10^{-3}$ kg m^2

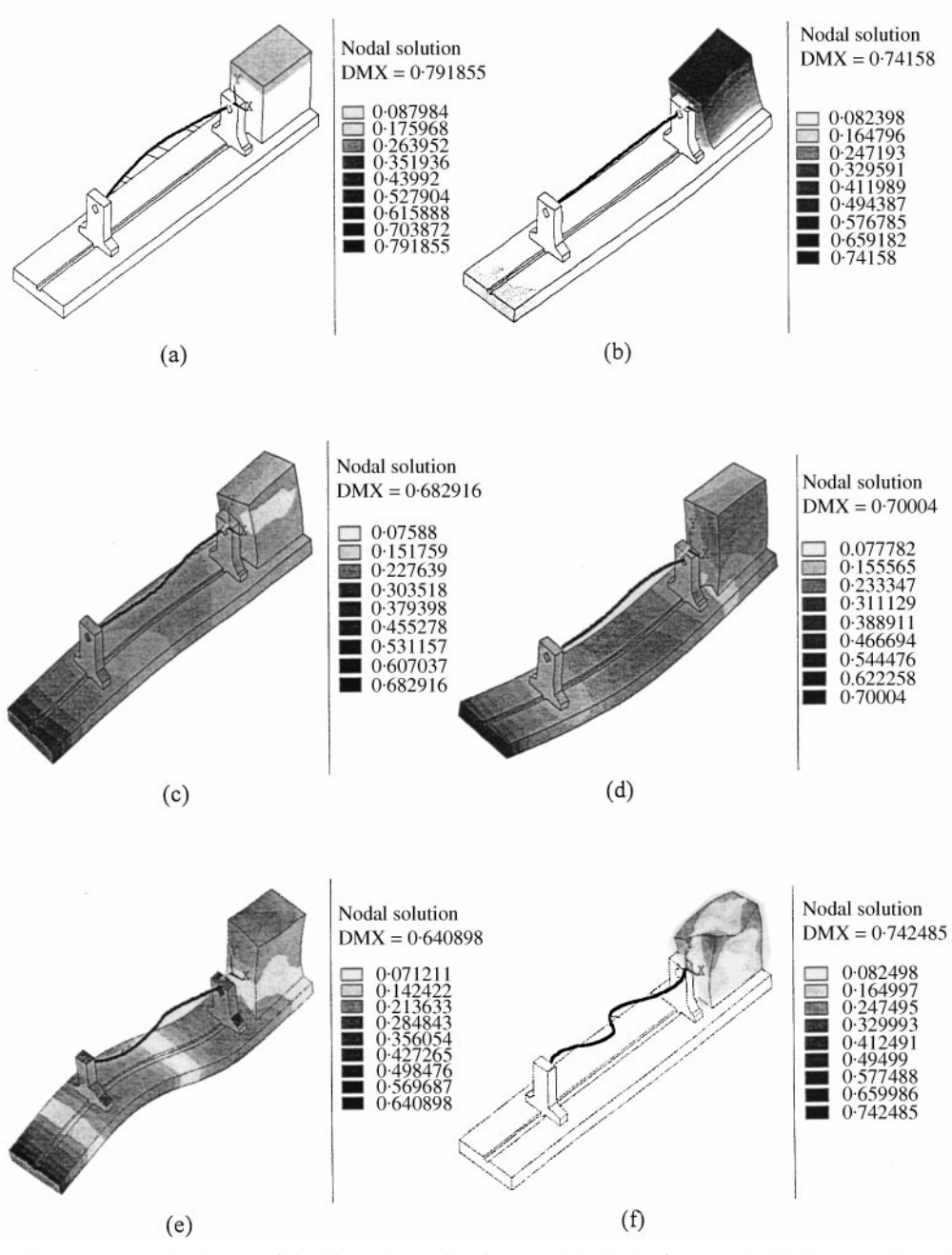

Figure. 22. Mode shapes of the kit as shown in Figure 21(a): (a) the first mode, (b) the second mode, (c) the third mode, (d) the fourth mode, (e) the fifth mode, (f) the sixth mode.

means of a FFT analyzer (HP3566A). The spectra of frequency responses from this transformation is generated and the natural frequencies of modes are calculated. Also, mode shapes of both kits are obtained from adopting the SIMO technique.

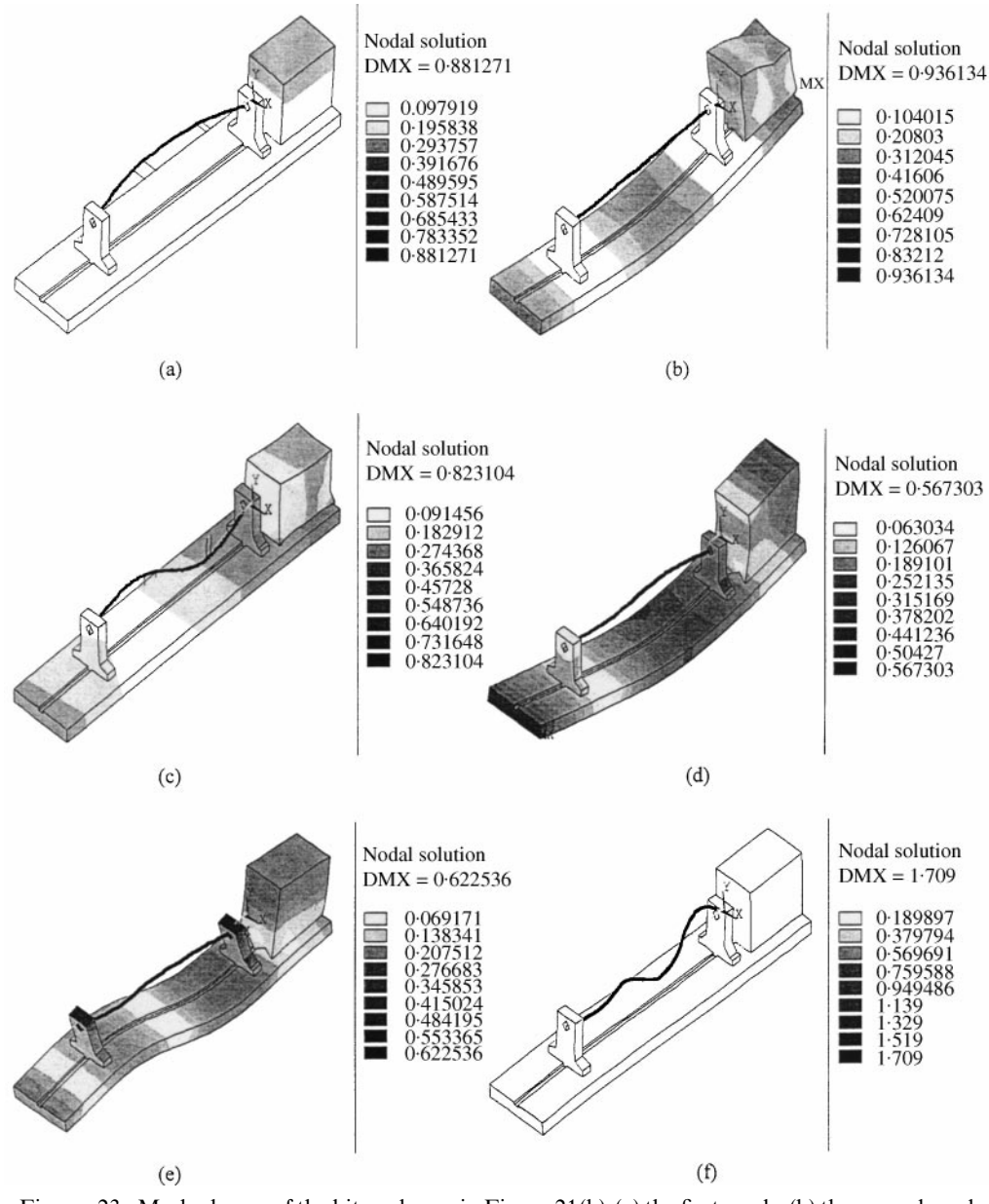

Figure. 23. Mode shapes of the kit as shown in Figure 21(b): (a) the first mode, (b) the second mode, (c) the third mode, (d) the fourth mode, (e) the fifth mode, (f) the sixth mode.

Natural frequencies resulting from modal testing and analytical simulation in these cases are listed in Table 5. From the comparison of data in this table, the errors of natural frequencies are observed to be within 5%.

The mode shapes of both systems are shown in Figures 22 and 23. These figures illustrate the deformations of rotor and foundation, in which gray-level distributions indicate the normalized displacements of the foundation.

TABLE 5

The comparison between analytical and experimental results of natural frequencies (Hz)

Mode	2-disk rotor			3-disk rotor		
	Testing	Simulation	Error (%)	Testing	Simulation	Error (%)
1	39·57	41·14	3·97	36·49	37·65	3·18
2	118·95	119·15	0·17	120·66	118·23	2·01
3	133·23	134·87	1·23	142·69	145·58	2·03
4	218·81	224·75	2·71	217·38	227·30	5·00
5	488·03	465·84	4·55	543·62	554·15	1·92

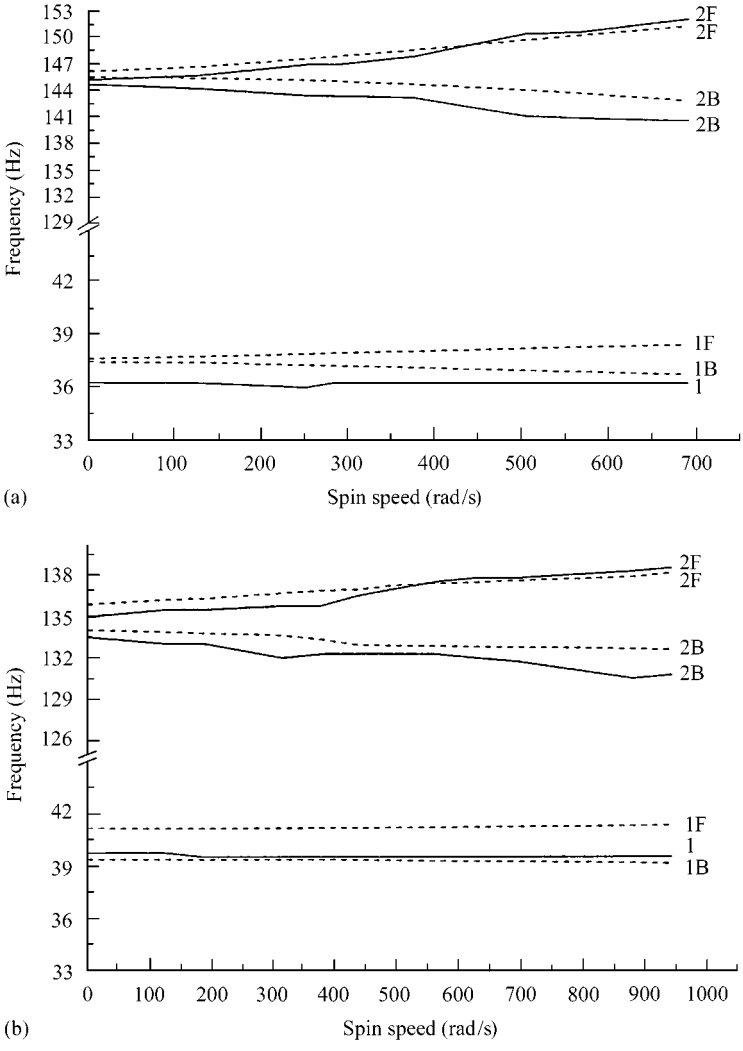

Figure. 24. Campbell diagrams depicting experimental results (——) and simulating results (- - - -): (a) three-disk kit; (b) two-disk kit.

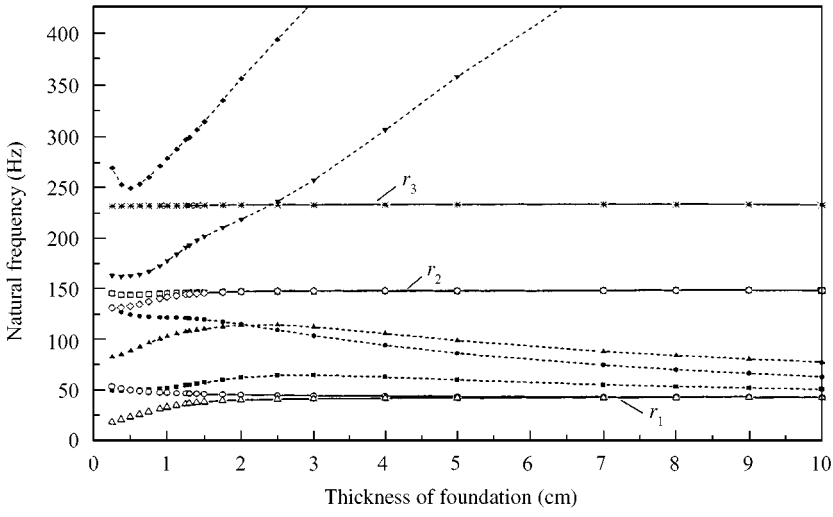

Figure. 25. Natural frequencies of the test kit with $K_b = 10^9$ N/m, $K_f = 8 \times 10^5$ N/m: —○—, 1st lateral mode (x) of rotor; —△—, 1st lateral mode (y) of rotor; —□—, 2nd lateral mode (x) of rotor; —◇—, 2nd lateral mode (y) of rotor; —∗—, torsional mode of rotor; – –■– –, 1st mode of foundation; – –▲– –, 2nd mode of foundation; – –●– –, 3rd mode of foundation; – –▼– –, 4th mode of foundation; – –◆– –, 5th mode of foundation.

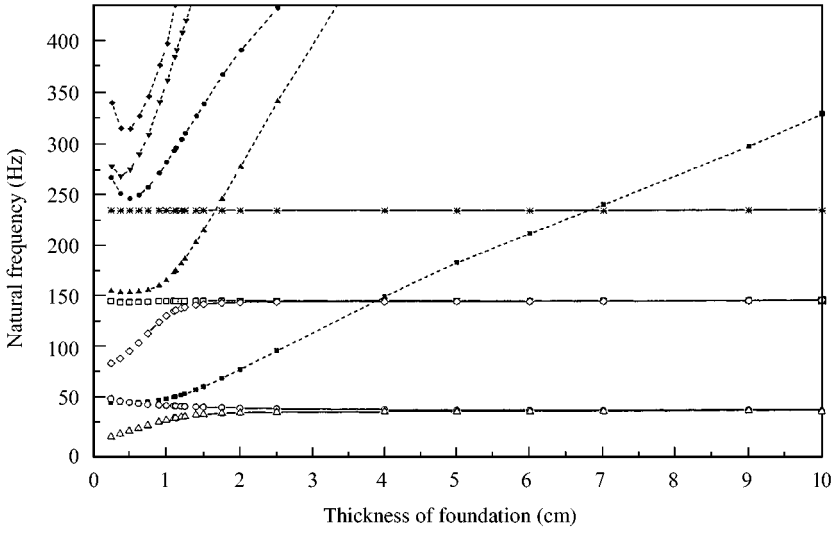

Figure. 26. Natural frequencies of the test kit with $K_b = K_f = 10^9$ N/m: —○—, 1st lateral mode (x) of rotor; —△—, 1st lateral mode (y) of rotor; —□—, 2nd lateral mode (x) of rotor; —◇—, 2nd lateral mode (y) of rotor; —∗—, torsional mode of rotor; – –■– –, 1st mode of foundation; – –▲– –, 2nd mode of foundation; – –●– –, 3rd mode of foundation; – –▼– –, 4th mode of foundation; – –◆– –, 5th mode of foundation.

Since that stiffness of foundation structure of these kits is anisotropic, the natural frequencies of forward and backward whirls do not arise from the same value at zero speed as shown in Figure 24. These Campbell diagrams produced by the analysis and the experiment of both kits have similar results.

Natural frequencies versus foundation thickness are shown in Figure 25, in which solid and dashed curves represent the modes of rotor and foundation respectively. The first three modes of foundation are rigid-body motions, and the frequencies decrease as thickness increases due to mass enlarging. Starting from the fourth mode, the natural frequencies of the foundation increase as the thickness increases due to the bending rigidity enlarging.

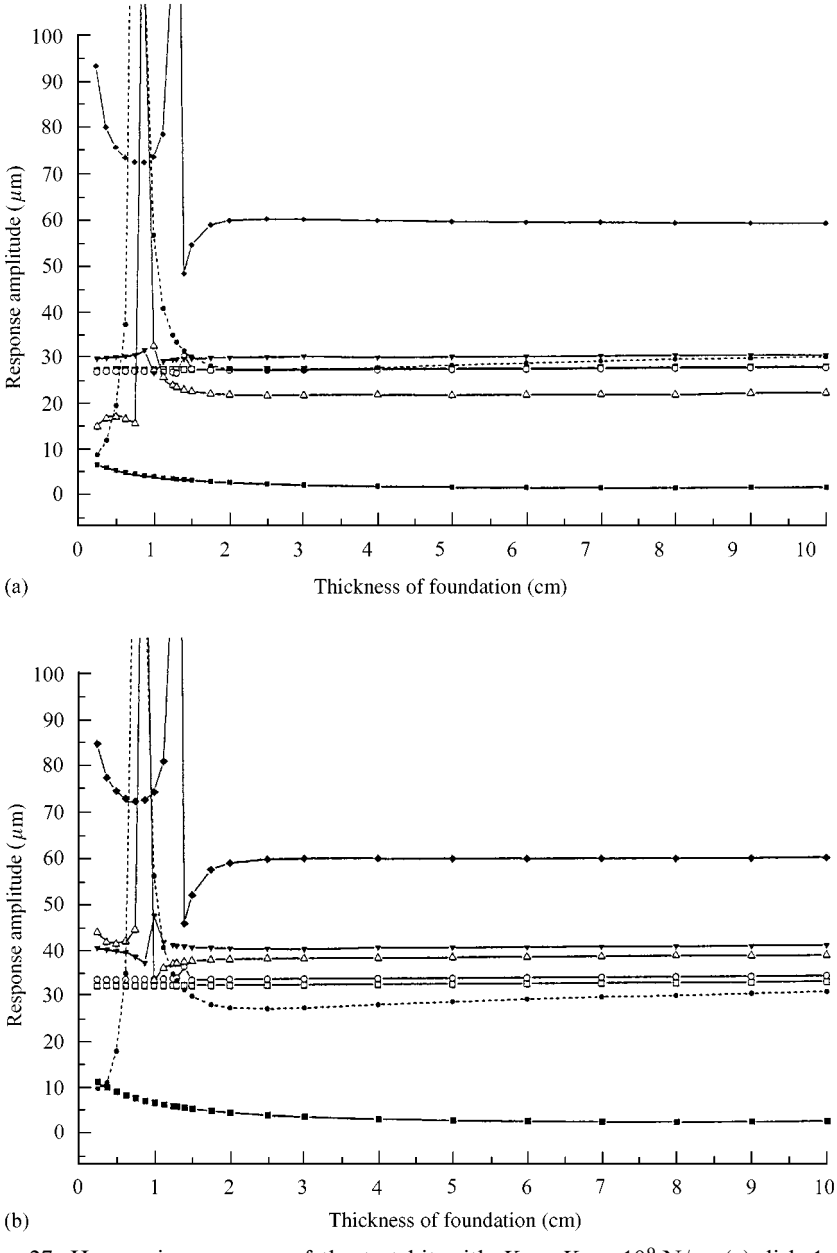

Figure. 27. Harmonic responses of the test kit with $K_b = K_f = 10^9$ N/m: (a) disk 1; (b) disk 2. —□—, spin speed 250 Hz; —○—, spin speed 200 Hz; —△—, spin speed 160 Hz; —▼—, spin speed 130 Hz; —◆—, spin speed 60 Hz; - - -■- - -, spin speed 30 Hz; —■—, spin speed 1 Hz.

For plate-type foundation, the natural frequencies of rotor modes increase as the plate thickness increases. When the thickness of foundation is appropriate, the natural frequencies tend to be steady no matter how the thickness changes. The natural frequencies $r_1 = 41{\cdot}78$ Hz, $r_2 = 145{\cdot}75$ Hz, $r_3 = 231{\cdot}90$ Hz are the first three modes of rotor-bearing system located at rigid ground and the stiffness coefficients of bearings are 10^9 N/m. Thus, the foundation is regarded as the rigid support of the rotor-bearing system when the foundation thickness is above 4 mm.

In this example, the appropriate foundation thickness is 3 mm at 200 Hz operating speed. Since the thickness is greater than 3 mm, there are six modes during a speed range within 200 Hz. If the thickness is less than 2 mm, there are eight modes within 200 Hz. When the operation speed is higher, the avoidance of the fourth mode of foundation must be considered. Thus, a greater thickness of foundation is required to raise the natural frequency of the fourth mode of foundation.

The rigid-body motion modes of foundation can be avoided if the foundation is mounted on a hard suspension, as shown in Figure 26. Also, this figure indicates that only one mode of foundation and three modes of rotor are within 400 Hz when the foundation thickness is greater than 3 mm. It can be observed that the available operating range is very wide. Thus, the natural frequencies of rotor are not influenced by stiffness coefficients of suspension. However, the natural frequencies of flexural modes of foundation increase as thickness increases. In Figures 25 and 26, the natural frequencies of rotor modes, which have similar mode shapes, are almost equal.

Further, the effects of thickness on the unbalance responses at some spin speeds are determined and shown in Figure 27. These speeds are 1, 30, 60, 130, 160, 200 and 250 Hz. When the foundation thickness is greater than 2 mm, the increase in thickness has no effect on the reduction of the unbalance responses.

9. CONCLUSION

This paper has extended the discussion on the foundation dynamics of the rotor-bearing system, in which three foundation types are considered. They are the lumped-mass foundation, the continuous-beam foundation, and the plate-type foundation. The analytical results and suggestions for foundation design as discussed in this paper can be summarized as follows:

1. When the suspension stiffness is soft, an increase in foundation mass decreases the natural frequencies of foundation modes. Thus, a hard suspension is selected preferably to avoid the rigid-body motion of the foundation within a given range of operating speed. For a hard suspension, an increase in foundation size raises the natural frequencies of modes and enlarges the range of operating speed.
2. For a soft structure of the foundation, the unbalance responses diminish and the natural frequencies of the rotor increase as the size of the foundation increases. When the structure of the foundation is stiff enough, the unbalance

responses cannot be suppressed and the natural frequencies of the rotor also cannot be raised as the size of the foundation increases. Hence, an appropriate stiffness of the foundation is acceptable.

3. An increase in a rotor's foundation size raises the natural frequencies of its flexural modes. If the rotor is operated at a high speed, a larger size foundation is needed to avoid flexural modes of itself in the operating range.

ACKNOWLEDGMENTS

This study was supported by the National Science Council, the Republic of China, under grant number NSC 84-2212-E033-013.

REFERENCES

1. R. G. Kirk and E. J. Gunter 1972 *ASME Journal of Engineering for Industries* 94, 221–232. The effect of support flexibility and damping on the synchronous response of a single-mass flexible rotor.
2. D. M. Smith 1933 *Proceedings of the Royal Society*, *Series A* **142**, 92. The motion of a rotor carried by a flexible shaft in flexible bearing.
3. J. W. Lund 1965 *Journal of Applied Mechanics*, Vol. 32, *Transations ASME*, *Series E* **87**, 911–920. The stability of an elastic rotor in journal bearings with flexible, damped supports.
4. E. J. Gunter 1967 *Journal of Engineering for Industry. Transactions ASME*, *Series B* **89**, 683–688. The influence of internal friction on the stability of high speed rotors.
5. J. W. Lund and B. Sternlicht, 1962 *Journal of Basic Engineering*, *Transactions ASME*, *Series D* **84**, 491–502. Rotor-bearing dynamics with emphasis on attenuation.
6. J. Dworski 1964 *Journal of Engineering for Power. Transactions ASME*, *Series A* **86**, 149–160. High speed rotor suspension formed by fully floating hydrodynamic radial and thrust bearings.
7. E. J. Gunter 1970 *Journal of Lubrication Technology*, *Transactions ASME*, *Series F* **92**, 59–75. Influence of flexibly mounted rolling element bearing on rotor response, Part I—linear analysis.
8. W. D. Pilkey, B. P. Wang and D. Vannoy 1976 *ASME Journal of Engineering for Industries* 1026–1029. Efficient optimal design of suspension systems for rotating shafts.
9. R. Gasch 1976 *Journal of Sound and Vibration* **47**, 53–73. Vibration of large turborotors in fluid-film bearing on an elastic foundation.
10. J. M. Vance, B. T. Murphy and H. A. Tripp 1987 *ASME Journal of Vibration Acoustics*, *Stress*, *Reliability in Design* **109**, 8–14. Critical speeds of turbomachinery: computer predictions vs. experimental measurements—Part II: effect of tilt-pad bearing and foundation dynamics.
11. R. W. Stephenson and K. E. Rouch 1992 *Journal of Sound and Vibration* **154**, 467–484. Generating matrices of the foundation structure of a rotor system from test data.
12. R. L. Ruhl and J. F. Booker 1972 *ASME Journal of Engineering for Industry* **94**, 126–132. A finite element models for distributed parameter turborotor systems.
13. H. D. Nelson and J. M. McVaugh 1976 *ASME Journal of Engineering for Industries* **98**, 593–600. The dynamics of rotor-bearing systems using finite elements.
14. E. S. Zorzi and H. D. Nelson 1977 *ASME Journal of Engineering for Power* **99**, 71–76. Finite element simulation of rotor-bearing systems with internal damping.
15. E. S. Zorzi and H. D. Nelson 1980 *ASME Journal of Mechanical Design* **102**, 158–161. The dynamics of rotor-bearing systems with axial torque—a finite element approach.

16. H. D. NELSON 1980 *ASME Journal of Mechanical Design* **102**, 793–803. A finite rotating shaft element using Timoshenko beam theory.
17. L. M. GREENHILL, W. B. BICKFORD and H. D. NELSON 1985 *ASME Journal of Vibration Acoustics, Stress, Reliability in Design* **107**, 421–430. A conical beam finite element for rotor dynamic analysis.
18. H. ÖZGÜVEN and L. Z. ÖZKAN 1984 *ASME Journal of Vibration, Acoustics, Stress, and Reliability in Design* **106**, 72–79. Whirl speeds and unbalance response of multi-bearing rotors using finite elements.
19. N. F. RIEGER 1976 *Machine Design* **22**, 89–95. A comprehensive guide to computer programs for analysis rotor systems.
20. R. FIROOZIAN and R. STANWAY 1989 *Journal of Sound and Vibration* **134**, 115–137. Design and application of a finite element package for modelling turbomachinery vibrations.
21. ANSYS Analysis Guides, Release 5.5, 1998, SAS IP, Inc., U.S.A.

APPENDIX A

The schematic diagram of a rotating disk is shown in Figure 2. The force and moment equilibrium of the disk can be derived from

$$
\begin{aligned}
F^d_{xi} &= m^d(\ddot{x}_i - \ddot{x}_j), \quad F^d_{xj} = m^d(\ddot{x}_j - \ddot{x}_i),\\
F^d_{yi} &= m^d(\ddot{y}_i - \ddot{y}_j), \quad F^d_{yj} = m^d(\ddot{y}_j - \ddot{y}_i),\\
M^d_{xi} &= I_x(\ddot{\theta}_{xi} - \ddot{\theta}_{xj}) + J\Omega(\dot{\theta}_{yi} - \dot{\theta}_{yj}),\\
M^d_{yi} &= I_y(\ddot{\theta}_{yi} - \ddot{\theta}_{yj}) - J\Omega(\dot{\theta}_{xi} - \dot{\theta}_{xj}),\\
M^d_{xj} &= I_x(\ddot{\theta}_{xj} - \ddot{\theta}_{xi}) + J\Omega(\dot{\theta}_{yj} - \dot{\theta}_{yi}),\\
M^d_{yj} &= I_y(\ddot{\theta}_{yj} - \ddot{\theta}_{yi}) - J\Omega(\dot{\theta}_{xj} - \dot{\theta}_{xi}),
\end{aligned} \tag{A1}
$$

where $F^d_{xj}, F^d_{yj}, F^d_{xi}, F^d_{yi}, M^d_{xi}, M^d_{yi}, M^d_{xj}, M^d_{yj}$ are components of interactive force and moment between a common node of shaft and disk.

Figure 3(a) shows a typical bearing model. By ignoring the length effect of the bearing, the linearized equilibrium of a bearing element is derived as

$$
\begin{aligned}
Q^b_{xi} &= K^b_{xx}(x_i - x_j) + K^b_{xy}(y_i - y_j) + C^b_{xx}(\dot{x}_i - \dot{x}_j) + C^b_{xy}(\dot{y}_i - \dot{y}_j),\\
Q^b_{yi} &= K^b_{yx}(x_i - x_j) + K^b_{yy}(y_i - y_j) + C^b_{yx}(\dot{x}_i - \dot{x}_j) + C^b_{yy}(\dot{y}_i - \dot{y}_j),\\
Q^b_{xj} &= K^b_{xx}(x_j - x_i) + K^b_{xy}(y_j - y_i) + C^b_{xx}(\dot{x}_j - \dot{x}_i) + C^b_{xy}(\dot{y}_j - \dot{y}_i),\\
Q^b_{yj} &= K^b_{yx}(x_j - x_i) + K^b_{yy}(y_j - y_i) + C^b_{yx}(\dot{x}_j - \dot{x}_i) + C^b_{yy}(\dot{y}_j - \dot{y}_i),
\end{aligned} \tag{A2}
$$

where Q^b_{xi}, Q^b_{yi} are interactive forces between the common node of shaft and bearing, and Q^b_{xj}, Q^b_{yj} are interactive forces between the common node of bearing and foundation.

As shown in Figure 3(b), the force equilibrium of connectors between the foundation and ground can be derived from

$$Q^s_{xi} = K^s_{xx}(x_i - x_j) + K^s_{xy}(y_i - y_j) + C^s_{xx}(\dot{x}_i - \dot{x}_j) + C^s_{xy}(\dot{y}_i - \dot{y}_j),$$

$$Q^s_{yi} = K^s_{yx}(x_i - x_j) + K^s_{yy}(y_i - y_j) + C^s_{yx}(\dot{x}_i - \dot{x}_j) + C^s_{yy}(\dot{y}_i - \dot{y}_j),$$

$$Q^s_{xj} = K^s_{xx}(x_j - x_i) + K^s_{xy}(y_j - y_i) + C^s_{xx}(\dot{x}_j - \dot{x}_i) + C^s_{xy}(\dot{y}_j - \dot{y}_i),$$

$$Q^s_{yj} = K^s_{yx}(x_j - x_i) + K^s_{yy}(y_j - y_i) + C^s_{yx}(\dot{x}_j - \dot{x}_i) + C^s_{yy}(\dot{y}_j - \dot{y}_i). \tag{A3}$$

where Q^s_{xi}, Q^s_{yi} are interactive forces between the common node of bearing and foundation, and Q^s_{xj}, Q^s_{yj} are interactive forces between the common node of foundation and ground.

APPENDIX B

As shown in Figure 4(b), the force equilibrium of the non-rotating support element is

$$-Q^i_b = K_b(q_i - q_f) + C_b(\dot{q}_i - \dot{q}_f) \tag{B1}$$

at the shaft end, and

$$Q^f_b = K_b(q_f - q_i) + C_b(\dot{q}_f - \dot{q}_i) \tag{B2}$$

at the foundation end. Thus,

$$\begin{aligned} m_f\ddot{q}_f &= -Q^f_b - K_f q_f - C_f\dot{q}_f + F_f \\ &= -(K_b - K_f)q_f + K_b q_i - (C_b + C_f)\dot{q}_f + C_b\dot{q}_i \end{aligned} \tag{B3}$$

is obtained by substituting equation (B2) into the force equilibrium of the foundation.

APPENDIX C: NOMENCLATURE

A	displacement amplitude
E	modulus of elasticity
F	force
$\{F\}$	the vector of external force
K	stiffness coefficient
C	damping coefficient
$[C]$, $[G]$	damping, gyroscopic matrix
I	the moment of area of foundation,
I_x, I_y, I_z	the moment of mass of disk with respect to x-, y-, and z axis
J	the torsional moment of inertia of disk

M	moment
$[M], [K]$	mass, stiffness matrix
m, m_f, m_r	mass, foundation mass, rotor mass
q	generalized co-ordinates
$\{q\}$	the vector of nodal displacements
Q	interactive force
$\{Q\}$	the vector of interactive force
u	nodal displacement
ρ	density
θ	nodal rotation
ω	natural frequency
ω_r	fundamental frequency of rotor-bearing system
Ω	rotating speed

Superscript

b	bearing
d	disk
e	shaft
f	foundation
g	ground
r	rotor
s	suspension

Subscript

a	all of the interior d.o.f. of rotor-bearing system
b	the interior d.o.f. between bearing and foundation
c	the interior d.o.f. of foundations
f	foundation
g	unidirectional load
i	the node of rotating support element
s	suspension
u	unbalance forces
x, y, z	co-ordinates axes